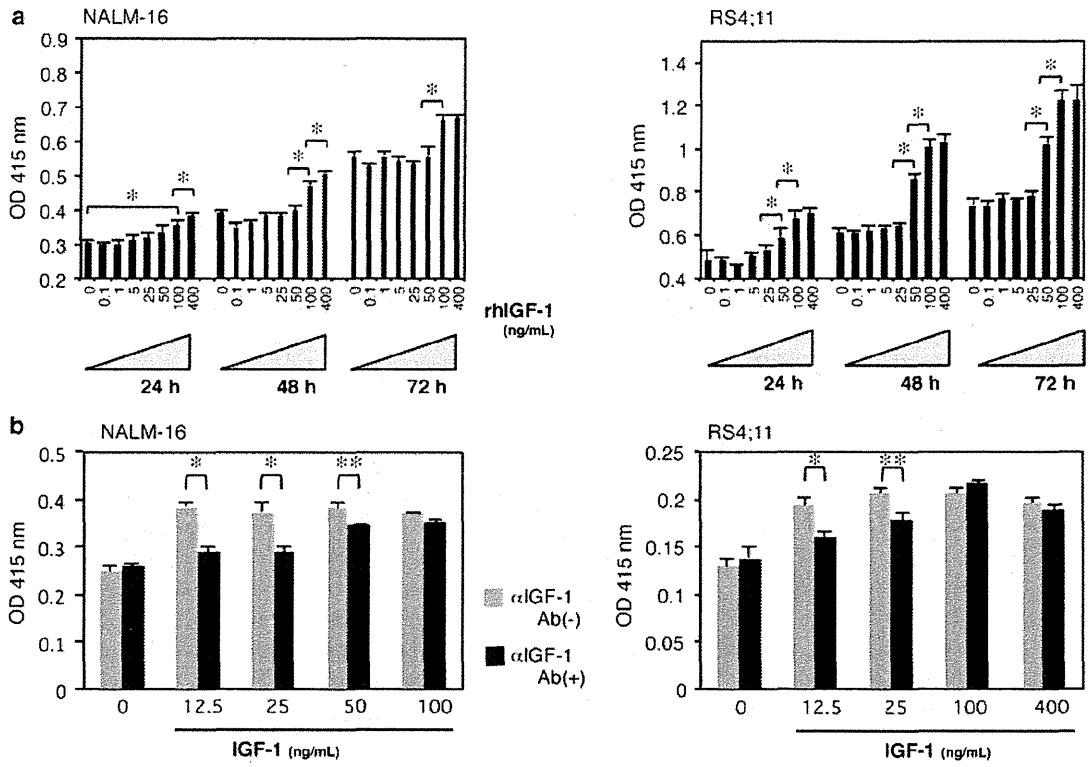

Fig. 3 Effect of insulin-like growth factor-1 (IGF-1) and anti-human IGF-1 antibody (αIGF-1Ab) on the proliferation of B-cell precursor acute lymphoblastic leukemia (BCP-ALL) cell lines. **a** NALM-16 and RS4;11 cells were cultured at a starting cell concentration of 5×10^5 and 2.5×10^5 cells/mL, respectively, with 0.5 % fetal calf serum (FCS) in the presence and absence of indicated concentrations of recombinant human IGF-1 for 72 h, and subsequent cell proliferations were assessed by WST assays. **b** The cells at the same starting cell concentration were cultured with 0.5 % FCS in the presence and absence of αIGF-1Ab (10 μg/ml) with or without IGF-1 at the indicated concentrations, and analyzed as in **a**. Each experiment was performed in triplicate, and the mean ± SD of the OD values are shown. Data are representative of at least three independent experiments. *significant ($p < 0.01$); **significant ($p < 0.05$)

10 % (v/v) fetal bovine serum (FBS; NescoHealthScience Pty, Ltd. Mexico) at 37 °C in a humidified 5 % CO_2 atmosphere.

Cell growth and apoptosis assay

Cells were cultured in the presence or absence of IGF-1, IGFBPs, anti-human IGF-1 antibody, and kinase inhibitors, as indicated in the figures and legends. For apoptosis induction, cells were cultured in the presence or absence of DEX and VP-16, or irradiated using a linear accelerator (Al 0.5 + Cu 0.3 mm filter, 1.27 Gy/min; MBR-1520R-3; Hitachi, Tokyo, Japan), as indicated in the figures and legends. Cell proliferations were assessed by either water-soluble tetrazolium salt (WST) assays (Cell Counting Kit-8, DojinDo, Kumamoto, Japan) or quantitative measurement of the adenosine 5′-triphosphate (ATP) levels using the luciferin–luciferase assay solution (TOYO B-Net CO., LTD., Tokyo, Japan) according to the manufacturer's protocol. In parallel, viable cell counts were made after staining with Trypan blue (Sigma Chemical Company, St. Louis, MO, USA). The frequency of apoptosis was quantified using the Annexin V-FITC Apoptosis Detection kit (BioVision, Milpitas, CA, USA) and then analyzed according to the manufacturer's protocol.

Immunofluorescence analysis

To detect IGF-1R expression, cells were stained with phycoerythrin (PE)-conjugated anti-IGF-1Rα antibody in combination with electron-coupled dye (ECD)-conjugated anti-CD45 antibody and analyzed by flow cytometry (FCM, FC500, Beckman), as described previously [19]. Analysis was done by collecting 10,000 gated list mode events, and selecting an appropriate blast gate for the combination of CD45 and side scatter. The IGF-1R was considered positively expressed when at least 20 % of the gated cells expressed IGF-1R. The cell cycle was assessed with the BrdU Flow Kit (Becton Dickinson Biosciences) and analyzed by flow cytometry according to the manufacturer's

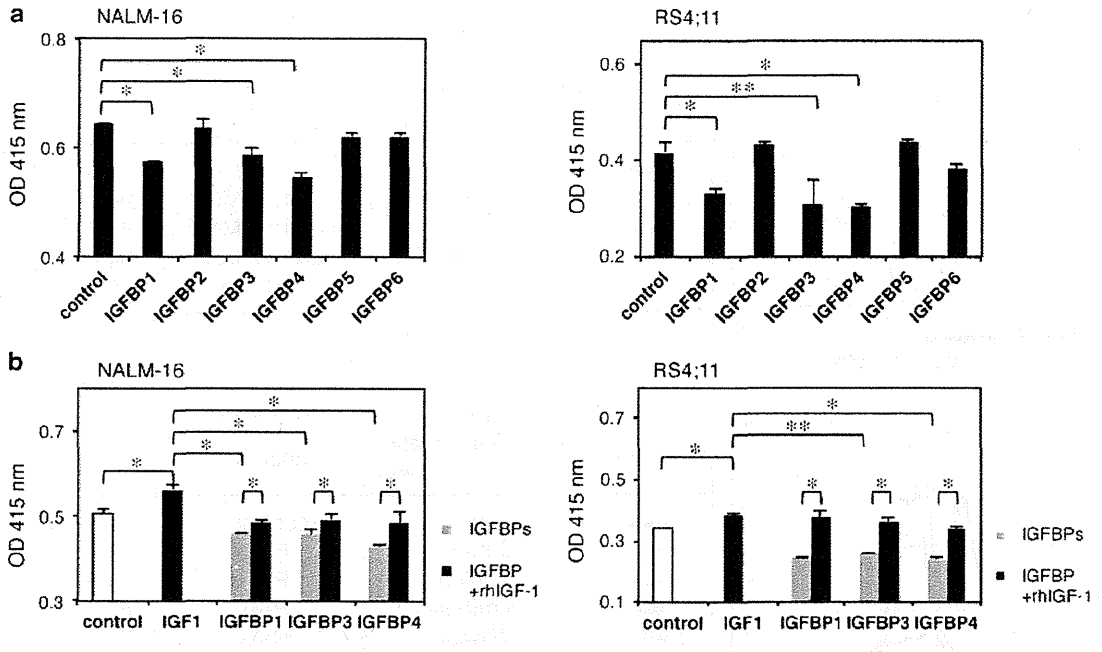

Fig. 4 Effect of insulin-like growth factor binding proteins (IGFBPs) on the proliferation of B-cell precursor acute lymphoblastic leukemia (BCP-ALL) cell lines. **a** Each IGFBP (at a concentration of 200 ng/mL) as indicated was added alone to the culture of NALM-16 (starting at cell concentration of 5×10^5 cells/mL with 0.5 % fetal calf serum) and RS4;11 [starting at cell concentration of 2.5×10^5 cells/mL with 10 % fetal calf serum (FCS)] and resulting cell proliferations after a 72-h cultivation were assessed by WST assay. The data are indicated as OD values. **b** IGFBP-1, -3, and -4 were added to the culture under the same experimental conditions as in **a** in the presence and absence of IGF-1 (100 ng/mL) and analyzed similarly to **a**. Each experiment was performed in triplicate, and the mean ± SD of the data are shown. Data are representative of at least three independent experiments. $*p < 0.01$; $**p < 0.05$

protocol. To detect phosphorylations of p44/42 MAPK and Akt, cells stimulated with IGF-1, as indicated in the figures and legends, were fixed with formaldehyde (final concentration: 2 %, room air temperature for 10 min), permeabilized with methanol (final concentration 90 %, −20 °C, 30 min), blocked with 0.5 % bovine serum albumin (room temperature for 10 min), and then incubation with phospho-specific Ab against each kinase (room temperature for 60 min), followed by FCM analysis.

Immunoblotting

Immunoblotting was performed as described previously [20]. Briefly, a 50-μg sample of each cell lysate was electrophoretically separated on an SDS-poly acrylamide gel and transferred to a nitrocellulose membrane. The membrane was incubated with an appropriate combination of primary and secondary Abs, washed, and examined with an enhanced chemiluminescence reagent system.

Statistical analysis

Statistical analysis was performed by means of a non-parametric Mann–Whitney test, and correlations were determined using nonparametric statistics. A p-value <0.05 was considered significant.

Results

Expression of IGF-1R in BCP-ALL cells

First, we examined whether the clinical materials of BCP-ALL cells expressed IGF-1R. As shown in Fig. 1a and b, five out of thirty-two cases apparently expressed IGF-1Rα (>50 %) and three cases weakly expressed IGF-1R. The frequency of positive IGF-1R expression (>20 %) of our cases was 25.0 %. On the other hand, when BCP-ALL cell lines were similarly examined, all of the cell lines expressed IGF-1Rα (Fig. 1c).

Effect of IGF-1 on cell proliferation of BCP-ALL cell lines

Using NALM-16 and RS4;11 cells, we next investigated the effect of IGF-1 on the cell cycle and proliferation of BCP-ALL cell lines. When cells treated with or without IGF-1 were examined by BrdU assay, IGF-1 stimulation increased the ratio of cells in the S phase and the cells in the G0/G1

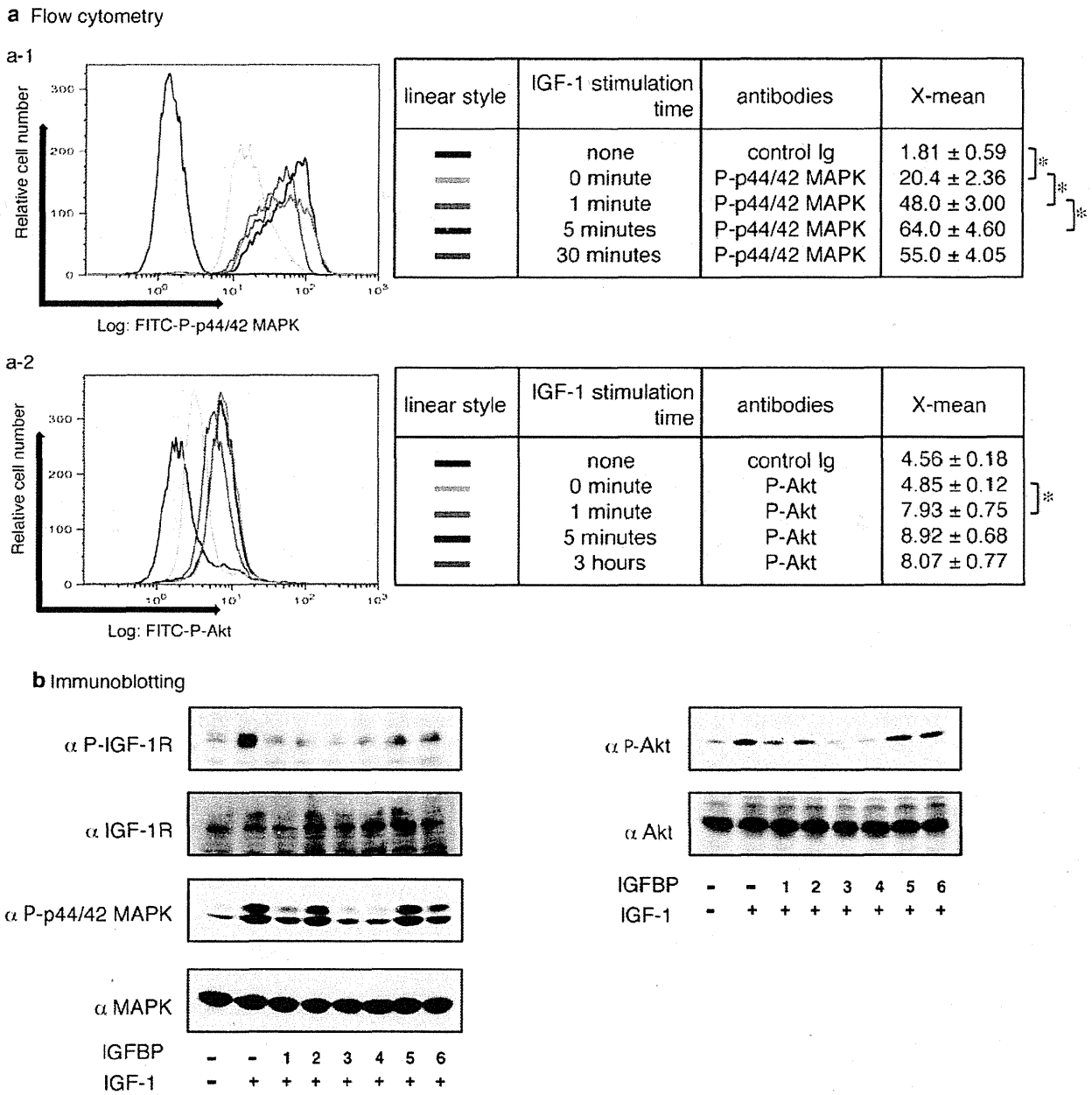

Fig. 5 Effects of insulin-like growth factor binding proteins (IGFBPs) on insulin-like growth factor-1 (IGF-1)-mediated signaling. **a** NALM-16 cells were stimulated with 100 ng/mL of IGF-1 under serum-free conditions for the indicated periods, and phosphorylations of p44/42 mitogen-activated protein kinase (MAPK) (*a-1*) and Akt (*a-2*) were detected by anti-phospho-specific antibodies using flow cytometry. Each experiment was performed in triplicate, and average mean fluorescence (X-mean) values are presented. Control Ig, staining with isotype-matched control rabbit Ig. Data are representative of at least three independent experiments. *X*-axis, fluorescence intensity; *Y*-axis, relative cell number. **b** NALM-16 cells were stimulated with 100 ng/mL of IGF-1 under serum-free conditions for 1 min in the presence and absence of 200 ng/mL each of IGFBP, as indicated. Cell extracts were prepared, and immunoblotting with indicated antibodies was performed. Data are representative of three independent experiments. *significant ($p < 0.01$)

phase decreased (Fig. 2). Then, we examined the proliferative effect of IGF-1 on BCP-ALL cell lines. As shown in Fig. 3a, the addition of IGF-1 leads to a dose-dependent increase in cell proliferation in each cell line and the concentration of 100 ng/ml had already achieved a maximum effect. Furthermore, when cell proliferation was inhibited by anti-IGF-1Ab, IGF-1 also had a recovery effect on cell proliferation in a dose-dependent manner (Fig. 3b).

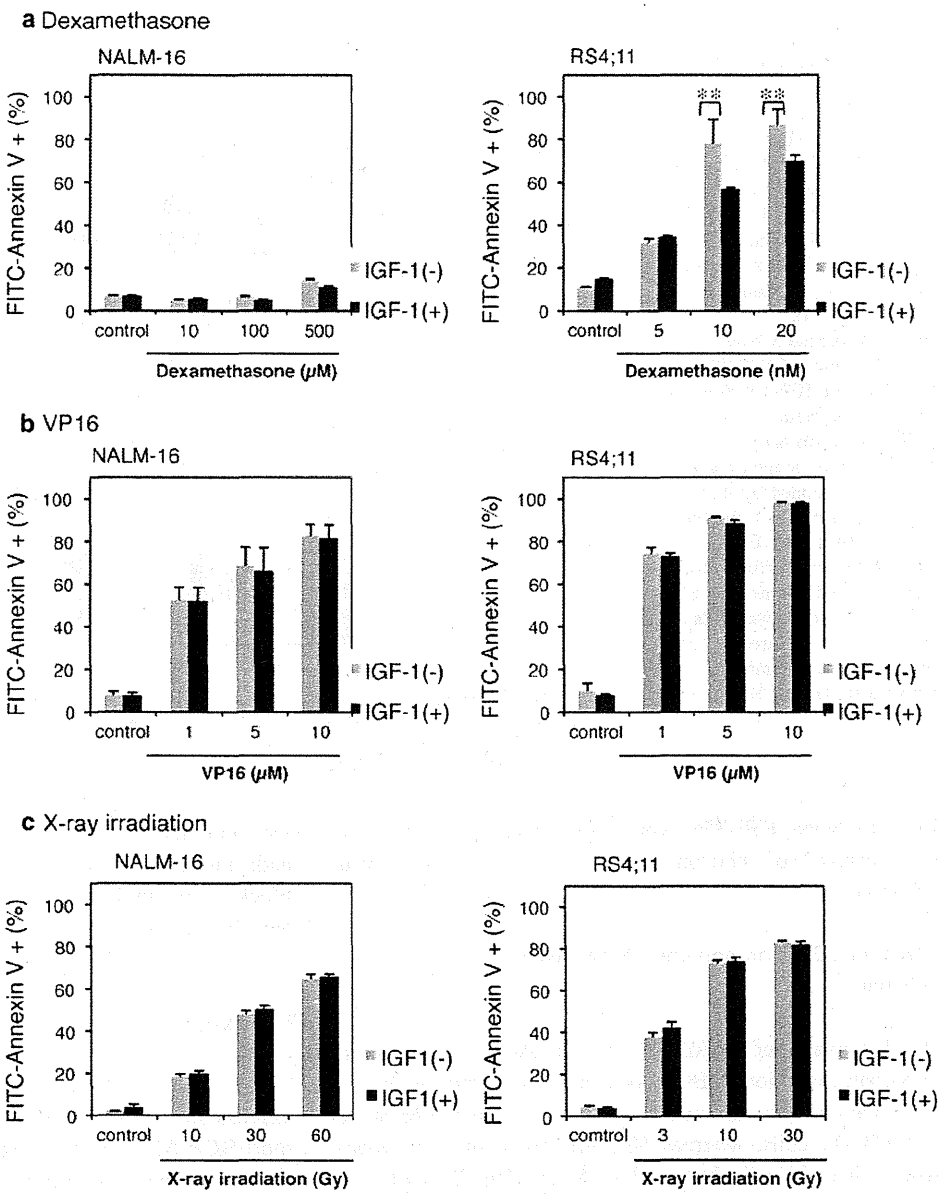

Fig. 6 Effect of insulin-like growth factor-1 (IGF-1) on apoptosis in B-cell precursor acute lymphoblastic leukemia (BCP-ALL) cell lines. NALM-16 and RS4;11 cells were cultured with or without the indicated doses of dexamethasone (**a**), VP16 (**b**), and irradiation (**c**), and the resulting apoptotic cells were examined by Annexin V-binding using flow cytometry. Each experiment was performed in triplicate, and the mean ± SD of the percentage of Annexin V-binding cells are presented. Data are representative of at least three independent experiments. **significant ($p < 0.05$)

Effect of IGFBPs on the proliferation of BCP-ALL cell lines

We then examined the effect of IGFBPs on IGF-1-mediated cell proliferation. As shown in Fig. 4a, when each IGFBP alone was added to the culture, IGFBP-1, -3, and -4 inhibited the cell proliferation. Inhibitions of the cell proliferation effect were reduced by the simultaneous addition of IGF-1, indicating that IGFBP-1, -3, and -4 specifically inhibited IGF-1-mediated cell proliferation (Fig. 4b).

IGF-1-mediated intracellular signaling in BCP-ALL cells

Subsequently, we investigated the IGF-1-mediated intracellular signaling in BCP-ALL cells. When the phosphorylation state of p44/42 MAPK and Akt induced by IGF-1-stimulation was examined by flow cytometry, a time-dependent increase in phosphorylation of these proteins was observed (Fig. 5a). The IGF-1-mediated enhancement of phosphorylation on IGF-1R, MAPK, and Akt was also confirmed by immunoblotting (Fig. 5b). As shown in

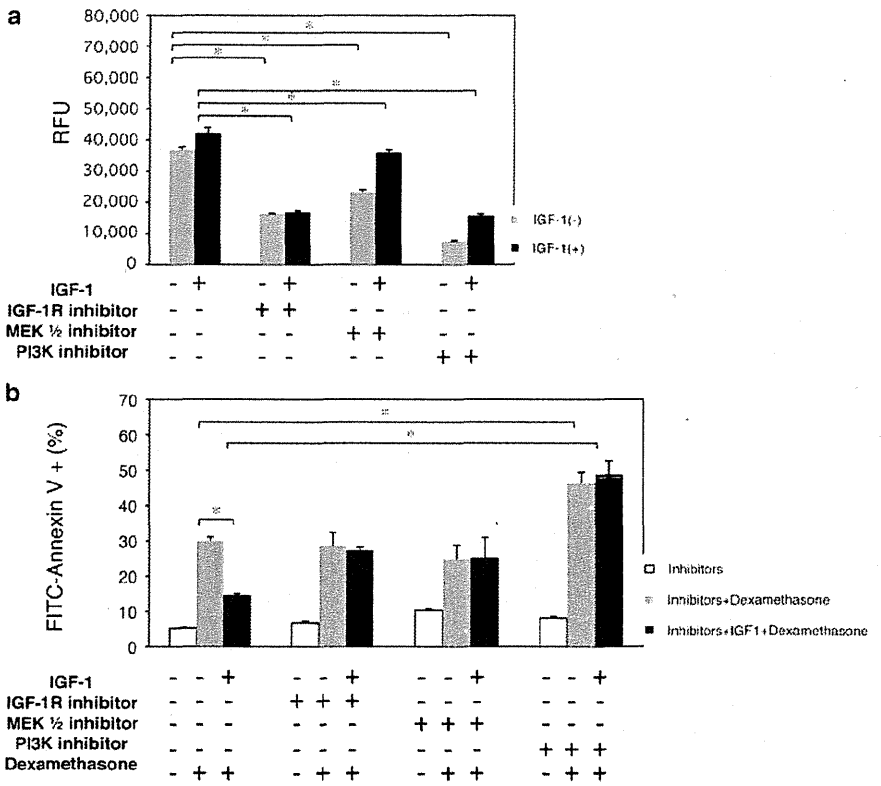

Fig. 7 Effect of inhibitors of insulin-like growth factor-1-related signaling molecules on the B-cell precursor acute lymphoblastic leukemia (BCP-ALL) cell line. RS4;11 cells were incubated with or without IGF-1R kinase inhibitor I-OMe-AG538 (50 μM), the mitogen-activated protein kinase extracellular signal-regulated kinase (MEK) 1/2 inhibitor U0126 (20 μM), phosphoinositide 3-kinase (PI3K) inhibitor LY294002 (50 μM), and IGF-1 100 ng/mL for 60 h and resulting cell proliferation (**a**) and the frequencies of apoptotic cells (**b**) were examined by ATP assay and Annexin V-binding assay, respectively. Each experiment was performed in triplicate, and the mean ± SD of the data are shown. Data are representative of three independent experiments. *significant ($p < 0.01$)

Fig. 5b, when IGF-BPs were added simultaneously, the enhancement of phosphorylation of each protein was inhibited.

Effect of IGF-1 on apoptosis induction of BCP-ALL cell lines

We then examined whether IGF-1-stimulation could inhibit apoptosis induction in BCP-ALL cells. As shown in Fig. 6, VP-16 and irradiation induced apoptosis in both NALM-16 and RS4;11 cells, whereas DEX-treatment induced apoptosis in RS4;11 cells, but not NALM-16 cells. When IGF-1 was added to the culture, apoptosis induced by DEX was partially inhibited, whereas apoptosis mediated by other treatments was not affected.

Next, we examined the effect of inhibitors for kinases. As mentioned above, stimulation of IGF-1R by the binding of IGF-1 is thought to be mainly mediated by MAPK and PI3K pathways. Although incubation with inhibitors for IGF-1R, MAPK, and Akt reduced cell proliferation, all of them induced apoptosis. When cells were incubated with a combination of IGF-1R inhibitor and IGF-1, the proliferative effect of IGF-1 was completely blocked, whereas, when cells were incubated with either MEK or Akt inhibitor, the proliferative effect of IGF-1 was only partially blocked. On the other hand, the inhibition of DEX-induced apoptosis mediated by IGF-1 was completely blocked by IGF-1R inhibitor (Fig. 7b). In addition, either MEK or Akt inhibitor also completely blocked the inhibition of DEX-induced apoptosis mediated by IGF-1.

Discussion

The results of the present study clearly showed the expression of IGF-1R by BCP-ALL cells. As we presented, most BCP-ALL cell lines expressed IGF-1R, whereas IGF-1R expression was limited in some cases of clinical samples. Although the precise reason for the inconsistency in the frequency of IGF-1R expression between cell lines and fresh ALL cells is unknown, it may be that IGF-1R expression is an advantage for cell growth and, thus, IGF-1R-positive cases tend to more frequently be able to be established as a cell line. Indeed, IGF-1 introduces BCP-ALL cells in the S phase of the cell cycle and promotes cell proliferation in a dose-dependent manner.

On the other hand, we showed that IGFBP-1, -3, and -4 inhibit IGF-1-mediated cell proliferation. Our data indicated that the presence of these IGFBPs inhibited intracellular signaling mediated by IGF-1. Therefore, it is most likely that these IGFBPs obstruct the binding of IGF-1 to IGF-1R and, thus, inhibit IGF-1 stimulation. However, a number of studies reported the possibility of a direct effect

of IGFBPs independent of IGF-1 function [16]. Further experiments need to be performed to clarify the precise mechanism of the effect of IGFBPs on IGF-1-mediated proliferation of BCP-ALL cells.

We also showed that IGF-1 partially inhibits apoptosis induced by DEX, whereas it did not affect apoptosis mediated by other causes, including VP-16 and irradiation. Our data indicate that the mechanism of apoptosis induction mediated by DEX and others might be different and IGF-1 stimulation can only overcome DEX-mediated apoptosis among the three causes of apoptosis. Since corticosteroid is a common drug for the treatment of ALL, it is possible that the expression of IGF-1R may affect the therapeutic response in BCP-ALL cells. Although previous studies reported no significant correlation between either gene expression of IGF system components in ALL cells or the serum IGF-1 level and prognosis [14, 21], more precise studies should be performed to evaluate the prognostic significance of IGF-1R expression in BCP-ALL cells.

Interestingly, both MEK inhibitor and Akt inhibitor completely blocked the inhibition of DEX-induced apoptosis mediated by IGF-1, while the proliferative effect of IGF-1 was only partially blocked by each inhibitor. Our data suggest that activation of both the MAPK and Akt pathways is required for the inhibition of DEX-induced apoptosis, whereas the activation of one of these pathways can support the proliferation of BCP-ALL cells, at least in part.

In conclusion, we observed IGF-1R expression in both clinical samples and cell lines of BCP-ALL cells that mediate cell proliferation and the anti-apoptotic effect against DEX. Although more detailed experiments are clearly needed, our findings indicate the possible involvement of the IGF-1 system in the proliferation and survival of some BCP-ALL cases, and may provide a model for investigating the molecular basis of the biological effect of IGF-1 on BCP-ALL cells. Since fully human antibody directed against IGF-1R is now clinically available [22], a new therapeutic strategy might be identified.

Acknowledgments We thank Dr. Y. Matsuo for generous gifting of cell lines. We also thank H. Yagi for her excellent experimental assistance. This work was supported by a grant from Health and Labour Sciences Research Grants (the 3rd-term comprehensive 10-year strategy for cancer control H22-011), the Japan Health Sciences Foundation for Research on Publicly Essential Drugs and Medical Devices (KHA1002), the Grant of National Center for Child Health and Development (22A-5), Grant-in-Aid for Young Scientists (B) (23791211), and the Advanced research for medical products Mining Programme of the National Institute of Biomedical Innovation (NIBIO, 10-41, -42, -43, -44, -45).

Conflict of interest We have no financial relationships or conflicts of interest related to this manuscript to declare.

References

1. Brzozowski AM, Dodson EJ, Dodson GG, Murshudov GN, Verma C, Turkenburg JP, et al. Structural origins of the functional divergence of human insulin-like growth factor-I and insulin. Biochemistry. 2002;41:9389–97.
2. De Meyts P, Whittaker J. Structural biology of insulin and IGF1 receptors: implications for drug design. Nat Rev Drug Discov. 2002;1:769–83.
3. Taniguchi CM, Emanuelli B, Kahn CR. Critical nodes in signalling pathways: insights into insulin action. Nat Rev Mol Cell Biol. 2006;7:85–96.
4. Zhao H, Grossman HB, Spitz MR, Lerner SP, Zhang K, Wu X. Plasma levels of insulin-like growth factor-1 and binding protein-3, and their association with bladder cancer risk. J Urol. 2003;169:714–7.
5. Ryan PD, Goss PE. The emerging role of the insulin-like growth factor pathway as a therapeutic target in cancer. Oncologist. 2008;13:16–24.
6. Hankinson SE, Willett WC, Colditz GA, Hunter DJ, Michaud DS, Deroo B, et al. Circulating concentrations of insulin-like growth factor-I and risk of breast cancer. Lancet. 1998;351:1393–6.
7. Hermanto U, Zong CS, Wang LH. Inhibition of mitogen-activated protein kinase kinase selectively inhibits cell proliferation in human breast cancer cells displaying enhanced insulin-like growth factor I-mediated mitogen-activated protein kinase activation. Cell Growth Differ. 2000;11:655–64.
8. Ma J, Pollak MN, Giovannucci E, Chan JM, Tao Y, Hennekens CH, et al. Prospective study of colorectal cancer risk in men and plasma levels of insulin-like growth factor (IGF)-I and IGF-binding protein-3. J Natl Cancer Inst. 1999;91:620–5.
9. Yu H, Spitz MR, Mistry J, Gu J, Hong WK, Wu X. Plasma levels of insulin-like growth factor-I and lung cancer risk: a case-control analysis. J Natl Cancer Inst. 1999;91:151–6.
10. Rohrmann S, Grote VA, Becker S, Rinaldi S, Tjønneland A, Roswall N, et al. Concentrations of IGF-I and IGFBP-3 and pancreatic cancer risk in the European prospective investigation into cancer and nutrition. Br J Cancer. 2012;106:1004–10.
11. Chan JM, Stampfer MJ, Giovannucci E, Gann PH, Ma J, Wilkinson P, Hennekens CH, et al. Plasma insulin-like growth factor-I and prostate cancer risk: a prospective study. Science. 1998;279:563–6.
12. Park SL, Setiawan VW, Kanetsky PA, Zhang ZF, Wilkens LR, Kolonel LN, et al. Serum insulin-like growth factor-I and insulin-like growth factor binding protein-3 levels with risk of malignant melanoma. Cancer Causes Control. 2011;22:1267–75.
13. Doepfner KT, Spertini O, Arcaro A. Autocrine insulin-like growth factor-I signaling promotes growth and survival of human acute myeloid leukemia cells via the phosphoinositide 3-kinase/Akt pathway. Leukemia. 2007;21:1921–30.
14. Vorwerk P, Wex H, Hohmann B, Mohnike K, Schmidt U, Mittler U. Expression of components of the IGF signalling system in childhood acute lymphoblastic leukaemia. Mol Pathol. 2002;55:40–5.
15. Pollak M. Insulin and insulin-like growth factor signalling in neoplasia. Nat Rev Cancer. 2008;8:915–28.
16. Hwa V, Oh Y, Rosenfeld RG. The insulin-like growth factor-binding protein (IGFBP) superfamily. Endocr Rev. 1999;20:761–87.
17. Stewart CE, Bates PC, Calder TA, Woodall SM, Pell JM. Potentiation of insulin-like growth factor-I (IGF-I) activity by an antibody: supportive evidence for enhancement of IGF-I bioavailability in vivo by IGF binding proteins. Endocrinology. 1993;133(3):1462–5.
18. Taguchi T, Takenouchi H, Matsui J, Tang WR, Itagaki M, Shiozawa Y, et al. Involvement of insulin-like growth factor-I

and insulin-like growth factor binding proteins in pro-B-cell development. Exp Hematol. 2006;34:508–18.
19. Kiyokawa N, Kokai Y, Ishimoto K, Fujita H, Fujimoto J, Hata JI. Characterization of the common acute lymphoblastic leukaemia antigen (CD10) as an activation molecule on mature human B cells. Clin Exp Immunol. 1990;79:322–7.
20. Kiyokawa N, Lee EK, Karunagaran D, Lin SY, Hung MC. Mitosis-specific negative regulation of epidermal growth factor receptor, triggered by a decrease in ligand binding and dimerization, can be overcome by overexpression of receptor. J Biol Chem. 1997;272:18656–65.
21. Mohnike KL, Kluba U, Mittler U, Aumann V, Vorwerk P, Blum WF. Serum levels of insulin-like growth factor-I, -II and insulin-like growth factor binding proteins -2 and -3 in children with acute lymphoblastic leukaemia. Eur J Pediatr. 1996;155:81–6.
22. Kolb EA, Gorlick R, Houghton PJ, Morton CL, Lock R, Carol H, et al. Initial testing (stage 1) of a monoclonal antibody (SCH 717454) against the IGF-1 receptor by the pediatric preclinical testing program. Pediatr Blood Cancer. 2008;50:1190–7.

Cancer Cell
Article

An Inv(16)(p13.3q24.3)-Encoded *CBFA2T3-GLIS2* Fusion Protein Defines an Aggressive Subtype of Pediatric Acute Megakaryoblastic Leukemia

Tanja A. Gruber,[1,6,8] Amanda Larson Gedman,[6] Jinghui Zhang,[2,8] Cary S. Koss,[1] Suresh Marada,[3] Huy Q. Ta,[6] Shann-Ching Chen,[7] Xiaoping Su,[2,25] Stacey K. Ogden,[3] Jinjun Dang,[6] Gang Wu,[2] Vedant Gupta,[1] Anna K. Andersson,[6] Stanley Pounds,[5] Lei Shi,[5] John Easton,[8] Michael I. Barbato,[8] Heather L. Mulder,[8] Jayanthi Manne,[8] Jianmin Wang,[4,8] Michael Rusch,[2,8] Swati Ranade,[24] Ramapriya Ganti,[6] Matthew Parker,[2] Jing Ma,[7] Ina Radtke,[6] Li Ding,[8,11] Giovanni Cazzaniga,[13] Andrea Biondi,[14] Steven M. Kornblau,[9] Farhad Ravandi,[10] Hagop Kantarjian,[10] Stephen D. Nimer,[15] Konstanze Döhner,[16] Hartmut Döhner,[16] Timothy J. Ley,[8,11,12] Paola Ballerini,[17] Sheila Shurtleff,[6] Daisuke Tomizawa,[20] Souichi Adachi,[21] Yasuhide Hayashi,[22] Akio Tawa,[23] Lee-Yung Shih,[18] Der-Cherng Liang,[19] Jeffrey E. Rubnitz,[1] Ching-Hon Pui,[1] Elaine R. Mardis,[8,11,12] Richard K. Wilson,[8,11,12] and James R. Downing[6,8,*]

[1]Department of Oncology
[2]Department of Computational Biology
[3]Department of Biochemistry
[4]Information Sciences
[5]Department of Biostatistics
[6]Department of Pathology
[7]Hartwell Center for Biotechnology and Bioinformatics
[8]St. Jude Children's Research Hospital, Washington University Pediatric Cancer Genome Project
St. Jude Children's Research Hospital, Memphis, TN 38105, USA
[9]Department of Blood and Marrow Transplantation
[10]Department of Leukemia
University of Texas MD Anderson Cancer Center, Houston, TX 77030, USA
[11]The Genome Institute at Washington University
[12]Siteman Cancer Center
Washington University School of Medicine, St. Louis, MO 63110, USA
[13]Centro Ricerca Tettamanti, Pediatric Clinic, University of Milan-Bicocca, 20052 Monza, Italy
[14]Pediatric Unit, University of Milan-Bicocca, San Gerardo Hospital, 20900 Monza, Italy
[15]Molecular Pharmacology and Chemistry Program, Sloan Kettering Institute, New York, NY 10065, USA
[16]Department of Internal Medicine III, University of Ulm, 89081 Ulm, Germany
[17]Laboratoire d'Hématologie, Hôpital A. Trousseau, 75012 Paris, France
[18]Division of Hematology-Oncology, Department of Internal Medicine, Chang Gung Memorial Hospital, Chang Gung University, Taipei 105, Taiwan
[19]Division of Pediatric Hematology Oncology, Mackay Memorial Hospital, Taipei 104, Taiwan
[20]Department of Pediatrics, Tokyo Medical and Dental University, Tokyo 113-8510, Japan
[21]Human Health Sciences, Graduate School of Medicine, Kyoto University, Kyoto 606-8501, Japan
[22]Department of Haematology/Oncology, Gunma Children's Medical Center, Shibukawa 377-8577, Japan
[23]Department of Pediatrics, National Hospital Organization Osaka National Hospital, Osaka 540-0006, Japan
[24]Pacific Biosciences, Menlo Park, CA 94025, USA
[25]Present address: Department of Bioinformatics and Computational Biology, University of Texas MD Anderson Cancer Center, Houston, TX 77030, USA
*Correspondence: james.downing@stjude.org
http://dx.doi.org/10.1016/j.ccr.2012.10.007

SUMMARY

To define the mutation spectrum in non-Down syndrome acute megakaryoblastic leukemia (non-DS-AMKL), we performed transcriptome sequencing on diagnostic blasts from 14 pediatric patients and validated our

Significance

Acute megakaryoblastic leukemia (AMKL) accounts for 10% of childhood acute myeloid leukemia (AML). Although AMKL patients with Down syndrome (DS-AMKL) have an excellent survival, non-DS-AMKL patients have an extremely poor outcome with a 3 year survival of less than 40%. With the exception of the t(1;22) seen in the majority of infants with non-DS-AMKL, little is known about the molecular lesions that underlie this leukemia subtype. Our results identified a fusion gene, *CBFA2T3-GLIS2*, that functions as a driver mutation in a subset of these patients. Importantly, pediatric patients with *CBFA2T3-GLIS2* expressing AMKL had inferior outcomes (5 year survival 34.3% versus 88.9%; p = 0.03), demonstrating that this lesion is a prognostic factor in this leukemia population.

findings in a recurrency/validation cohort consisting of 34 pediatric and 28 adult AMKL samples. Our analysis identified a cryptic chromosome 16 inversion (inv(16)(p13.3q24.3)) in 27% of pediatric cases, which encodes a CBFA2T3-GLIS2 fusion protein. Expression of CBFA2T3-GLIS2 in *Drosophila* and murine hematopoietic cells induced bone morphogenic protein (BMP) signaling and resulted in a marked increase in the self-renewal capacity of hematopoietic progenitors. These data suggest that expression of CBFA2T3-GLIS2 directly contributes to leukemogenesis.

INTRODUCTION

Acute megakaryoblastic leukemia (AMKL) accounts for approximately 10% of pediatric acute myeloid leukemia (AML) and 1% of adult AML (Athale et al., 2001; Barnard et al., 2007; Oki et al., 2006; Tallman et al., 2000). AMKL is divided into two subgroups: AMKL arising in patients with Down syndrome (DS-AMKL), and leukemia arising in patients without Down syndrome (non-DS-AMKL). Although DS-AMKL patients have an excellent prognosis with an ~80% survival, non-DS-AMKL patients do not fare as well, with a reported survival of only 14%–34% despite high-intensity chemotherapy (Athale et al., 2001; Barnard et al., 2007; Creutzig et al., 2005). With the exception of the t(1;22) seen in infant non-DS-AMKL, little is known about the molecular lesions that underlie this leukemia subtype (Carroll et al., 1991; Lion et al., 1992; Ma et al., 2001; Mercher et al., 2001).

We recently reported data from a high-resolution study of DNA copy number abnormalities (CNAs) and loss of heterozygosity on pediatric de novo AML (Radtke et al., 2009). These analyses demonstrated a very low burden of genomic alterations in all pediatric AML subtypes except AMKL. AMKL cases were characterized by complex chromosomal rearrangements and a high number of CNAs. To define the functional consequences of the identified chromosomal rearrangements in non-DS-AMKL, the St. Jude Children's Research Hospital-Washington University Pediatric Cancer Genome Project performed transcriptome and exome sequencing on diagnostic leukemia samples.

RESULTS

AMKL Is Characterized by Chimeric Transcripts

Transcriptome sequencing was performed on diagnostic leukemia cells from 14 pediatric non-DS-AMKL patients (discovery cohort) (see Tables S1 and S2 available online). Our analysis identified structural variations (SVs) that resulted in the expression of chimeric transcripts encoding fusion proteins in 12 of 14 cases (Table S3). Remarkably, in 7 of 14 cases, a cryptic inversion on chromosome 16 (inv(16)(p13.3q24.3)) was detected that resulted in the joining of *CBFA2T3*, a member of the ETO family of nuclear corepressors, to *GLIS2*, a member of the GLI family of transcription factors (Figures 1, 2, and S1). In six of these cases, exon 10 of *CBFA2T3* was fused to exon 3 of *GLIS2*, whereas in the remaining one case, exon 11 of *CBFA2T3* was fused to exon 1 of *GLIS2*. Both encoded proteins retain the three CBFA2T3 N-terminal *nervy* homology regions that mediate protein interactions and the five GLIS2 C-terminal zinc finger domains that bind the *Glis* DNA consensus sequence (Figures 1A and 1B). Whole-genome sequence analysis of tumor and germline DNA from four cases demonstrated that the *CBFA2T3-GLIS2* chimeric gene resulted from simple balanced inversions in three cases and a complex rearrangement involving chromosomes 16 and 9 in the fourth case (Figures 2 and S1).

Chimeric transcripts were also detected in five of seven leukemia samples that lacked expression of *CBFA2T3-GLIS2*, including one case each expressing in-frame fusions of *GATA2-HOXA9*, *MN1-FLI1*, *NIPBL-HOXB9*, *NUP98-KDM5A*, *GRB10-SDK1*, and *C8orf76-HOXA11AS* (Figure 3; Table S3). Importantly, several of the genes involved in these translocations play a direct role in normal megakaryocytic differentiation (*GATA2* and *FLI1*), have been previously shown to be involved in leukemogenesis (*HOXA9*, *MN1*, *HOXB9*, *NUP98*, *KDM5A*), or are highly expressed in hematopoietic stem cells or myeloid/megakaryocytic progenitors (Figure S2) (Argiropoulos and Humphries, 2007; Buijs et al., 2000; Heuser et al., 2011; Kawada et al., 2001; Visvader et al., 1995; Wang et al., 2009). Analysis of a recurrency/validation cohort consisting of diagnostic leukemia cells from 62 AMKL cases (34 pediatric and 28 adult) revealed 6 additional pediatric samples carrying *CBFA2T3-GLIS2* for an overall frequency of 27% (13 of 48) in pediatric AMKL (Table S1). None of the adult AMKL cases contained this chimeric transcript, suggesting that this lesion is restricted to pediatric non-DS-AMKLs. *NUP98-KDM5A* was the only other chimeric transcript that was recurrent, being detected in 8.3% (4 of 48) of pediatric cases (Table S1). This chimeric transcript was also not detected in adult AMKLs.

Cooperating Lesions in AMKL

In addition to the described chimeric transcripts, exome sequence analysis on 10 of the 14 samples in the discovery cohort that had matched germline DNA, coupled with CNAs detected by Affymetrix SNP6 microarrays, revealed an average of 5 (range 1–14) somatic nonsilent sequence mutations and 5 (range 0–11) CNAs involving annotated genes per case. (Tables S4, S5, and S6; Figure S1). Despite the relative paucity of somatic mutations, recurrent lesions were identified in *JAK* kinase genes, *MPL* and *GATA1*, which have been previously shown to play a role in AMKL (Malinge et al., 2008). Sequence analysis of these genes in cases within the recurrency cohort that had available genomic DNA revealed activating mutations in *JAK* kinases (9 of 51, 17.6%) and *MPL* (2 of 51, 3.9%), as well as inactivating mutations in *GATA1* (5 of 51, 9.8%) (Tables S1 and S6). In addition, 7 of 14 cases with available copy number data contained amplification of chromosome 21 in the Down syndrome critical region (DSCR; chr21q22) that includes genes known to play a role in AML such as *RUNX1*, *ETS2*, and *ERG* (Table S4; Figure S1). Three of these cases carry the *CBFA2T3-GLIS2* chimeric gene. Importantly, the total burden of somatic mutations was significantly lower in the *CBFA2T3-GLIS2*-expressing cases (7.17 ± 3.60 versus 16.60 ± 5.13; $p = 0.009$; Table S5).

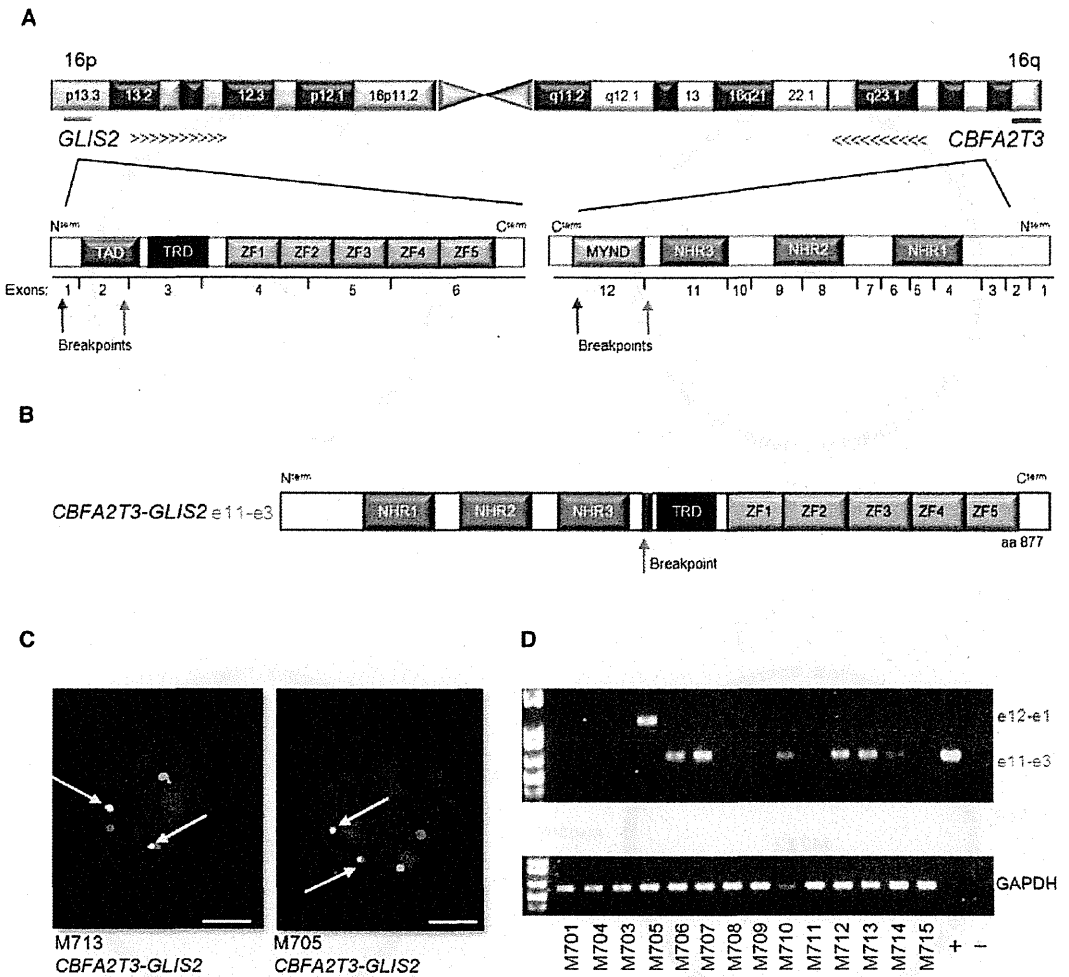

Figure 1. Inv(16)(p13.3;q24.3) Encodes a *CBFA2T3-GLIS2* Chimeric Transcript

(A) Schematic of chromosome 16 with locations of *GLIS2* and *CBFA2T3* shown. Arrows indicate orientation of the gene and the green and red lines the probes used for FISH. The protein structure of the genes is shown below chromosome 16 and is not drawn to scale. Breakpoints are indicated by arrows. TAD, transactivation domain; TRD, transcriptional regulatory domain; ZF, zinc finger; NHR, nervy homology region.

(B) Schematic of CBFA2T3-GLIS2 chimeric protein.

(C) Interphase FISH analysis of two representative patient samples carrying *CBFA2T3-GLIS2*. The *GLIS2* probe is green; the *CBFA2T3* probe is red. White arrows indicate the fusion event. Scale bars, 10 μm.

(D) RT-PCR for CBFA2T3-GLIS2 and GAPDH on the discovery cohort.

See also Figure S1 and Tables S1, S2, S3, S4, S5, and S6.

CBFA2T3-GLIS2 AMKL Is a Distinct Subtype of Pediatric AMKL with a Poor Prognosis

The gene expression profile of *CBFA2T3-GLIS2* AMKL was distinct from that of AMKL cells lacking this chimeric transcript and from other genetic subtypes of pediatric AML (Figures 4A and 4B). A detailed coexpression network analysis of the top 4,000 differentially expressed genes suggests that expression of *CBFA2T3-GLIS2* leads to marked upregulation of *BMP2*, a downstream target of Hedgehog signaling (Figures 4B and S3; Table S7). Moreover, gene set enrichment analysis based on KEGG pathway annotation of the top-scoring network module demonstrated Hedgehog and JAK-STAT pathways to be significantly upregulated in *CBFA2T3-GLIS2*-positive AMKL (Figure S3).

Given the historically poor outcomes seen in pediatric non-DS-AMKL, we next explored whether the presence of *CBFA2T3-GLIS2* identified a clinically distinct subset of cases. Outcome data were available on 40 pediatric patients. Although these patients were treated at a number of different centers using a variety of different therapeutic approaches, the presence of *CBFA2T3-GLIS2* identified a subgroup of patients with a significantly worse overall survival at 5 years as compared to patients with AMKL that lacked this chimeric transcript (28.1% versus 41.9%; p = 0.05; Figure 4C). Moreover, when this analysis was limited to patients treated at a single institution (St. Jude, n = 19), the adverse prognostic impact of *CBFA2T3-GLIS2* on survival was maintained (34.3% versus 88.9%; p = 0.03; Figure 4D).

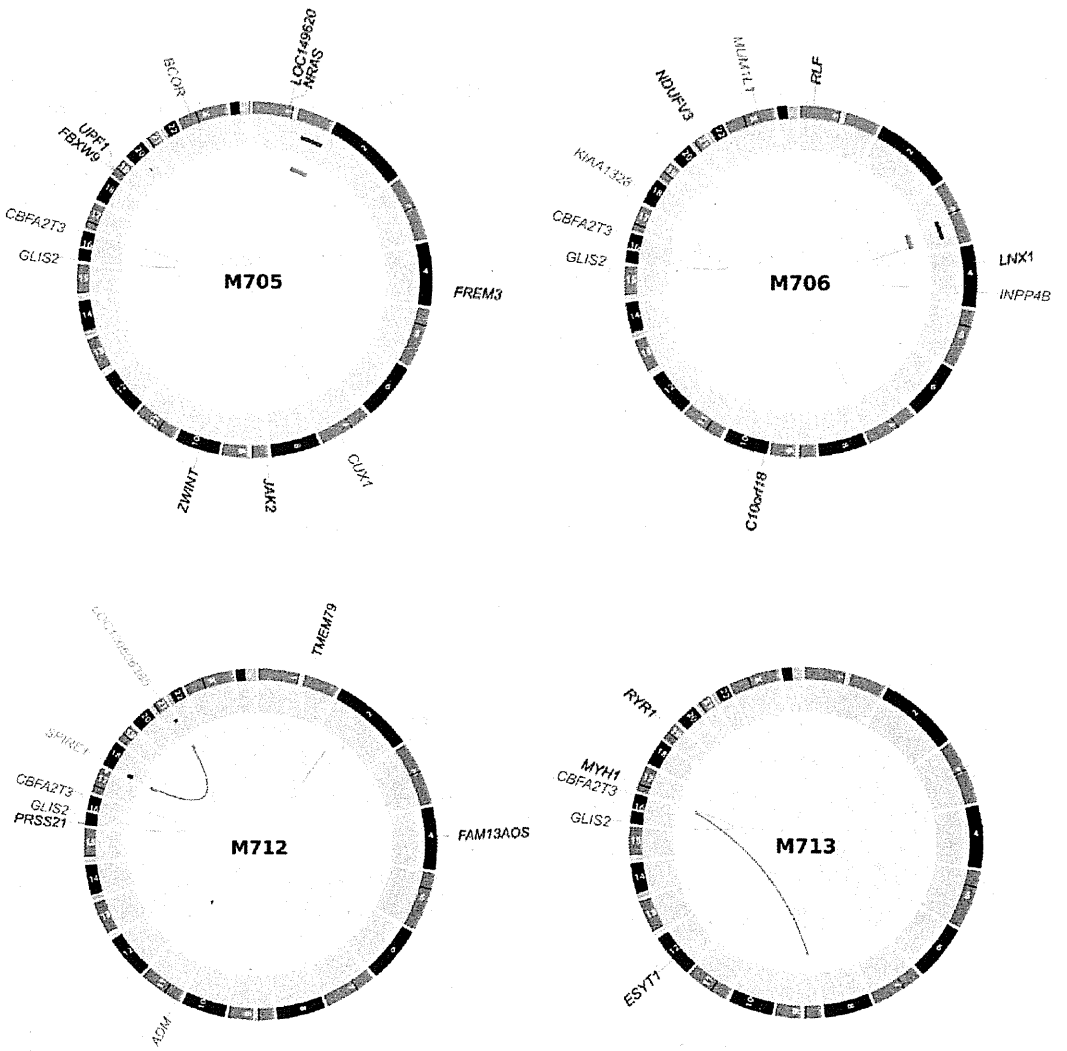

Figure 2. Somatic Mutations in Whole-Genome-Sequenced AMKL Cases

Plots depict structural genetic variants, including DNA copy number alterations, intra- and interchromosomal translocations, and sequence alterations (Krzywinski et al., 2009). DNA copy number alterations: loss of heterozygosity (LOH), orange; amplification, red; deletion, blue. Sequence mutations in Refseq genes: silent SNVs (SNVs), black; UTR, brown; nonsilent SNVs, blue. Genes at structural variant breakpoints: genes involved in in-frame fusions, red; others, green.

CBFA2T3-GLIS2-Modified Hematopoietic Cells Demonstrate Enhanced Self-Renewal

CBFA2T3 (also known as *MTG16*) was initially identified as a fusion partner with *RUNX1* in rare cases of therapy-related AML that contain a t(16;21)(q24;q22) (Gamou et al., 1998). More recently, CBFA2T3 has been implicated in the maintenance of hematopoietic stem cell quiescence (Chyla et al., 2008). By contrast, to our knowledge, GLIS2 has not been previously implicated in leukemogenesis. GLIS2 is a member of the GLI-similar (GLIS1-3) subfamily of Krüppel-like zinc finger transcription factors and is closely related to the GLI family of transcription factors that function as critical elements of the hedgehog signaling pathway (Kim et al., 2007; Lamar et al., 2001). GLIS2 is expressed in the kidney, and germline-inactivating mutations lead to nephronophthisis, an autosomal recessive cystic kidney disease (Attanasio et al., 2007). Although *GLIS2* is not normally expressed in the hematopoietic system, its fusion to *CBFA2T3* as a result of the inv(16)(p13.3q24.3) results in high-level expression of the C-terminal portion of the protein including its DNA-binding domain (Figure S1).

To explore the functional effects of the CBFA2T3-GLIS2 fusion protein, we transduced murine hematopoietic cells with a retrovirus expressing either *CBFA2T3-GLIS2* or *GLIS2* alone and assessed their effect on in vitro colony formation, differentiation, and replating efficiency as a surrogate measure of self-renewal (Figures 5A and 5B). On the initial plating, the expression of CBFA2T3-GLIS2 had no effect on colony numbers, size, or overall myeloid/erythroid differentiation when cells were grown in the presence of IL3, IL6, SCF, and EPO. However, hematopoietic cells transduced with the empty

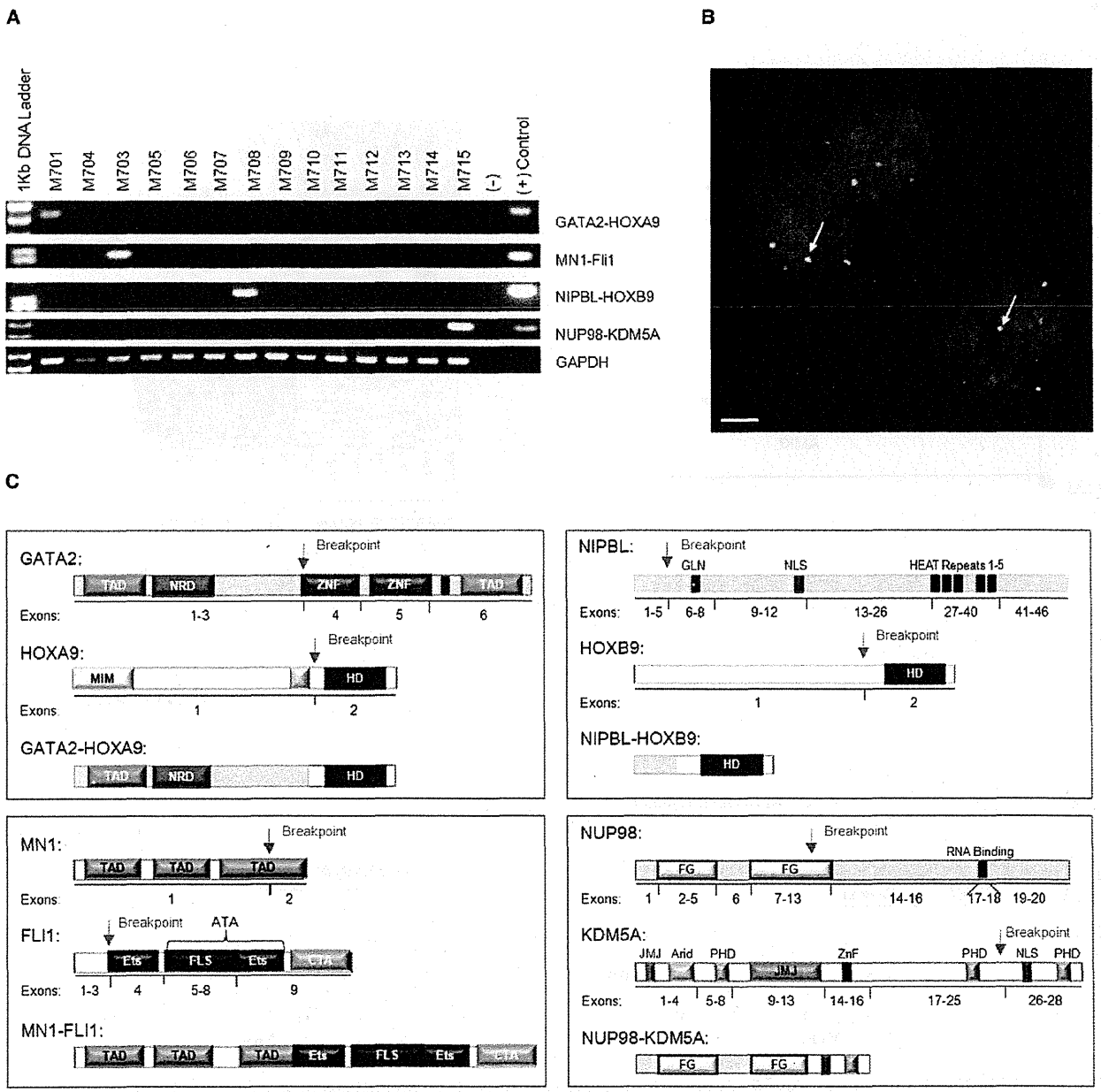

Figure 3. Low-Frequency Chimeric Transcripts in Pediatric AMKL

Four chimeric transcripts were identified in one case each of the discovery cohort and tested for in the recurrency cohort: *GATA2-HOXA9*, *MN1-FLI1*, *NIPBL-HOXB9*, and *NUP98-KDM5A*.

(A) RT-PCR validation of the discovery cohort. Primers and conditions are described in Supplemental Experimental Procedures.

(B) Interphase FISH analysis of M703 carrying the MN1-FLI1 chimeric protein. The *MN1* probe is red; the *FLI1* probe is green. White arrows indicate the fusion event. Scale bar, 10 μm.

(C) Schematic of chimeric proteins. Exons and domains are not drawn to scale. NRD, negative regulatory domain; ZNF, zinc finger; MIM, Meis interaction motif; HD, Hox domain; Ets, E-twenty six domain; FLS, Fli1-specific region; CTA, C-terminal transactivation domain; GLN, glutamine-rich domain; NLS, nuclear-localizing signal; HEAT, *H*untingtin/*E*F3/PP2*A*/*T*OR1 domain; FG, phenylalanine-glycine repeats; JMJ, jumonji domain; ARID, AT-rich interaction domain; PHD, plant homeodomain. See also Figure S2.

retrovirus (MSCV-IRES-mCherry [MIC]) failed to form colonies after the second replating, whereas expression of either CBFA2T3-GLIS2 or wild-type GLIS2 resulted in a marked increase in the self-renewal capacity, with colony formation persisting through ten replatings (Figure 5C). Upon serial replating, two colony types were detected: CFU-GM and CFU-Meg

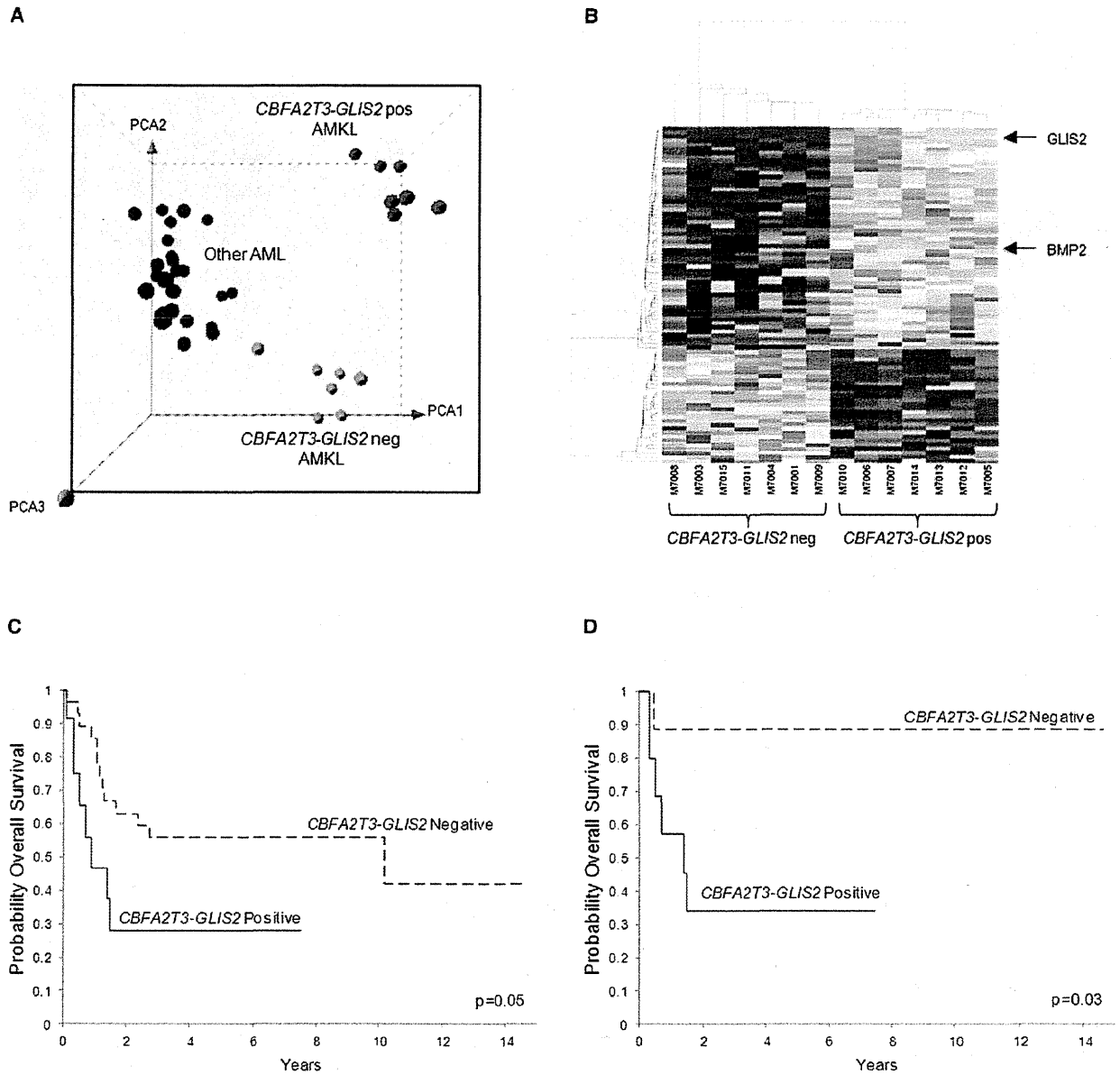

Figure 4. *CBFA2T3-GLIS2* Defines a Unique Subtype of AML with a Distinct Gene Expression Signature and Poor Outcomes

(A) Principal component analysis of the gene expression profiles of the AMKL discovery cohort and 32 other non-AMKL AML samples representing all other known genetic subtypes of pediatric AML. Clusters were generated using 1,000 genes selected by k-means algorithm. A detailed description of the samples included in this analysis can be found at NCBI Gene Expression Omnibus, accession GSE35203.

(B) Heatmap of differentially expressed genes in the top-scoring network module of CBFA2T3-GLIS2-positive (pos) and -negative (neg) AMKL patient samples. For gene relationships, please see Figure S3. For a detailed list of the top 500 differentially expressed genes (not limited to this network), please see Table S7.

(C) Overall survival of 40 pediatric non-DS AMKL cases treated at multiple institutions (*CBFA2T3-GLIS2*-negative cases n = 28, and *CBFA2T3-GLIS2*-expressing cases, n = 12). The curves for the two groups were tested by log rank method and exact test using permutation that yielded a p value of 0.05.

(D) Overall survival of 19 pediatric non-DS AMKL cases treated at St. Jude Children's Research Hospital (*CBFA2T3-GLIS2*-negative cases, n = 9, and *CBFA2T3-GLIS2*-expressing cases, n = 10). The curves for the two groups were tested by log rank method and exact test using permutation that yielded a p value of 0.03. See also Figure S3 and Table S7.

(Figure 5D). Immunophenotypic analysis at the third replating also revealed evidence of megakaryocytic differentiation with CD41/CD61 dual expression and the absence of cKIT and Sca1 expression in the majority of cells (Figure 5E). Importantly, CBFA2T3-GLIS2-expressing cells remained growth factor dependent, suggesting that cooperating mutations in growth factor

signaling pathways are likely required for full leukemic transformation (data not shown). Moreover, transplantation of *CBFA2T3-GLIS2*-transduced bone marrow cells into syngeneic recipients failed to induce overt leukemia at day 365 as demonstrated by normal blood counts and low-level reporter gene expression in peripheral blood (<5%) (data not shown), consistent with a requirement for cooperative mutations. Failure to induce leukemia in mice as a single lesion has been previously reported for other chimeric genes that confer the ability to serially replate in colony-forming assays, including *AML1-ETO* (Higuchi et al., 2002).

CBFA2T3-GLIS2 Induces BMP Signaling

GLIS2 can function as both a transcriptional activator and repressor depending on the cellular context and has been implicated in altered signaling through a number of pathways including sonic hedgehog-GLI1 (SHH) and WNT/β-catenin (Attanasio et al., 2007; Kim et al., 2007). Analysis of the gene expression signatures of *CBFA2T3-GLIS2* expressing AMKLs revealed altered expression of a number of genes in the SHH and WNT pathways, as well as genes in the bone morphogenic protein (BMP) pathway, which is directly influenced by SHH signaling (Figures 4B, 6A, and S3) (Dahn and Fallon, 2000; Ingham and McMahon, 2001; Vokes et al., 2007). When this analysis was limited to genes containing GLI consensus DNA-binding sites (Gli-BS) in their promoters or to genes known to be transcriptional targets of GLIS2, marked overexpression of *PTCH1*, *HHIP*, *BMP2*, and *BMP4* was observed (Figures 6B, S3, and S4; Table S7) (Attanasio et al., 2007). Consistent with this observation, although CBFA2T3-GLIS2 only weakly activated transcription of a reporter construct containing the Gli-BS (Figure S4), it strongly activated transcription of the Gli-BS-containing BMP4 promoter-driven luciferase construct and induced expression of BMP4 in murine hematopoietic cells (Figures 6C and S4). Moreover, CBFA2T3-GLIS2 strongly activated a BMP response element (BRE) containing luciferase reporter construct and induced expression of the BMP downstream transcriptional target, inhibitor of differentiation 1 (*ID1*) (Korchynskyi and ten Dijke, 2002), consistent with the induced expression of BMP2/BMP4 (Figure S4).

BMP signaling plays a critical role in the specification of hematopoiesis in developing embryos, and studies suggest that BMP4 stimulation can augment megakaryocytic output from CD34 progenitors (Jeanpierre et al., 2008; Söderberg et al., 2009). To determine if the observed CBFA2T3-GLIS2-induced BMP expression contributes to the enhanced replating capacity of murine hematopoietic cells, colony-replating assays were repeated in the presence of dorsomorphin, a selective small molecule inhibitor of the BMP type I receptors that blocks BMP-mediated phosphorylation of SMAD 1/5/8 (Yu et al., 2008). Importantly, CBFA2T3-GLIS2 as well as GLIS2-expressing hematopoietic cells were significantly more sensitive to dorsomorphin than wild-type cells in the first plating (Figure 6D). Continuous exposure to dorsomorphin inhibited colony formation in a dose-dependent manner on subsequent platings (data not shown). Interestingly, sublethal doses of dorsomorphin in *CBFA2T3-GLIS2*-positive cells led to an upregulation of *Bmp4* and *Id1* transcripts over time, with colony counts returning to untreated levels, suggesting that cells are able to overcome this inhibition by upregulating the BMP pathway (data not shown).

To further explore the downstream signaling of CBFA2T3-GLIS2 in human leukemia cell lines, we first assessed the expression level of *GLIS2* in human cancer cell lines using the recently published Broad-Novartis Cancer Cell Line Encyclopedia (Figure 7A) (Barretina et al., 2012). Interestingly, this analysis showed that GLIS2 expression levels are lowest in leukemia cell lines. Moreover, within the leukemias, the highest expressing cell line was the pediatric AMKL cell line M07e. To further explore AMKL cell lines, we performed RT-PCR for *CBFA2T3-GLIS2* on five human AMKL cell lines. Three of the five cell lines (RS1, WSU-AML, and M07e) expressed *CBFA2T3-GLIS2* (Figure 7B). The presence of the chimeric gene in these lines was validated by FISH analysis (Figure 7B). We went on to determine the relative expression of BMP genes by semiquantitative RT-PCR and found a trend toward upregulation of these genes in the CBFA2T3-GLIS2-positive cells (Figure 7C). We also assessed our AMKL cell lines for dorsomorphin sensitivity and found a trend toward increased sensitivity in cell lines expressing *CBFA2T3-GLIS2* as determined by a standard MTT assay (Figure 7D).

To determine if CBFA2T3-GLIS2 induces the upregulation of BMP signaling in vivo, we generated transgenic *Drosophila* expressing either *CBFA2T3-GLIS2* or full-length *GLIS2* using an epithelial promoter and examined their effect on fly development. During *Drosophila* development, the WNT, BMP, and SHH homologs (Wg, Dpp, and Hh, respectively) have distinct roles in patterning adult wing structures (Dahn and Fallon, 2000; Ingham and McMahon, 2001; Vokes et al., 2007). When altered, these signaling pathways trigger characteristic loss- and gain-of-function phenotypes (Tabata and Takei, 2004). Expression of CBFA2T3-GLIS2 and full-length GLIS2 in *Drosophila* resulted in ectopic expression of endogenous *dpp*, the fly homolog of *BMP4*, in wing imaginal discs (Figures 8A and S5). Immunofluorescence confirmed the nuclear localization of CBFA2T3-GLIS2 (Figure 8A). Both CBFA2T3-GLIS2 and GLIS2 overexpression induced lethality. However, a small number of escapers developed to pharate adults and demonstrated a morphologic *dpp* gain-of-function phenotype; wing hinges were converted to notum, and legs were shortened and broadened (Figure 8B) (Grieder et al., 2009). Rare *CBFA2T3-GLIS2* transgenic flies developed to adulthood and demonstrated mild ectopic venation throughout the wing blade, as well as wing blistering consistent with a *dpp* gain-of-function phenotype (Figure 8B) (Sander et al., 2010).

DISCUSSION

Sequence analysis of pediatric non-DS-AMKLs revealed the expression of an inv(16)-encoded *CBFA2T3-GLIS2* in almost 30% of pediatric non-DS-AMKL patients, and its presence defined a distinct subgroup of patients that had an exceptionally poor outcome when compared to patients with AMKL that lacked this lesion. In addition, five other chimeric transcripts (*GATA2-HOXA9*, *MN1-FLI1*, *NIPBL-HOXB9*, *GRB10-SDK1*, and *C8orf76-HOXA11AS*) were detected in single AMKL cases. Surprisingly, none of the identified chimeric transcripts was detected in adult AMKL cases, highlighting the significant

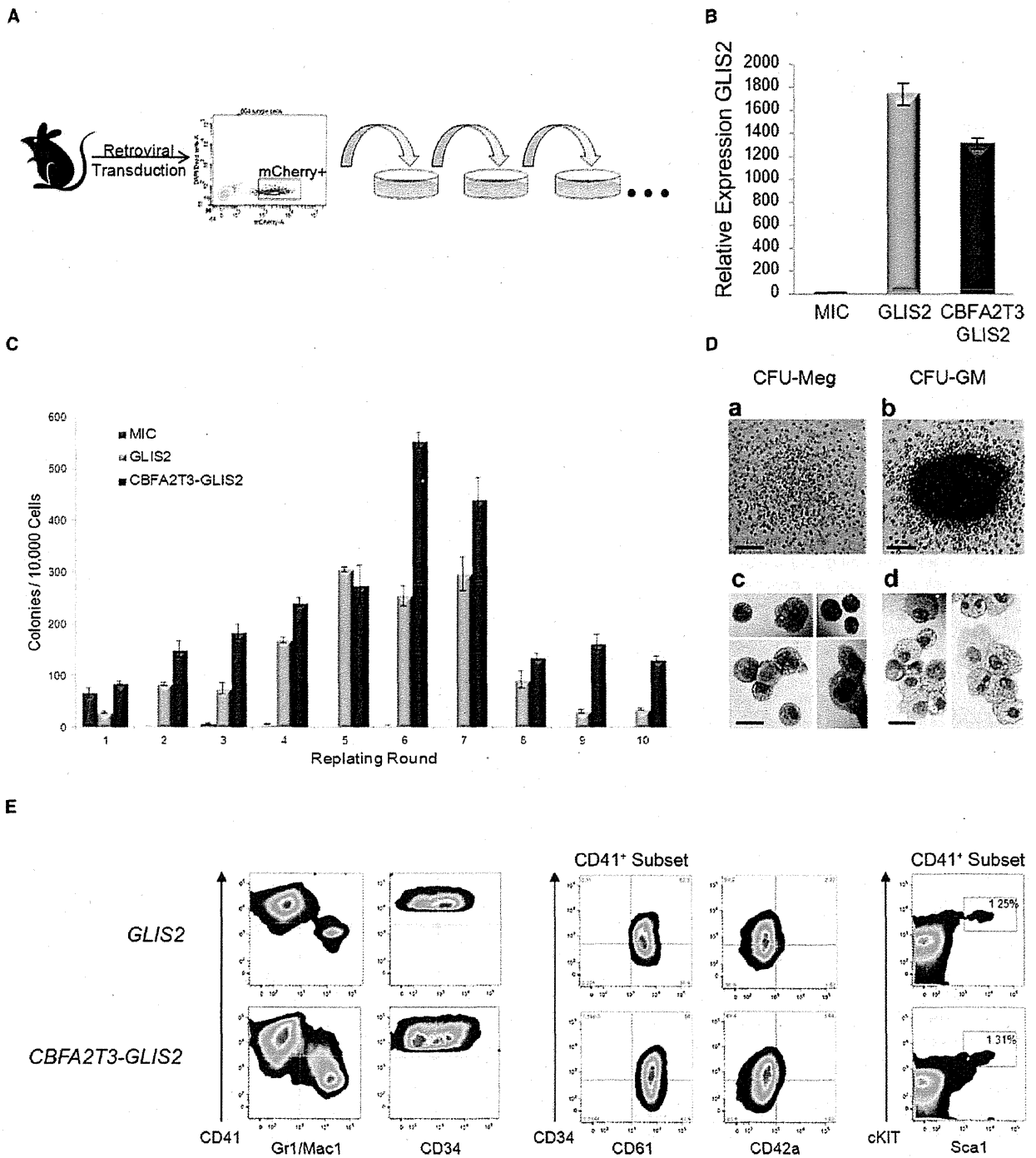

Figure 5. *CBFA2T3-GLIS2* Leads to Enhanced Replating of Hematopoietic Cells

(A) Experimental design. Murine bone marrow cells were transduced with retroviral vectors expressing mCherry alone (MIC), or mCherry along with *GLIS2*, or *CBFA2T3-GLIS2*. Transduced cells were purified by sorting mCherry-positive cells and plated onto methylcellulose containing IL3, IL6, SCF, and EPO. Colonies were counted after 7 days of growth and replated serially.

(B) Semiquantitative RT-PCR of GLIS2 utilizing cells harvested from first round of plating. *GLIS2* primers are specific for the 3′ half of the transcript and thus pick up both full-length GLIS2 as well as CBFA2T3-GLIS2. Expression in MIC cells was defined as one (1), and data are pooled from two separate experiments with similar results. $p \leq 0.0001$ as determined by one-way ANOVA. Error bars represent mean ± SEM of two independent experiments.

(C) Number of colonies detected at 7 days following each plating. Error bars represent mean ± SEM of two independent experiments.

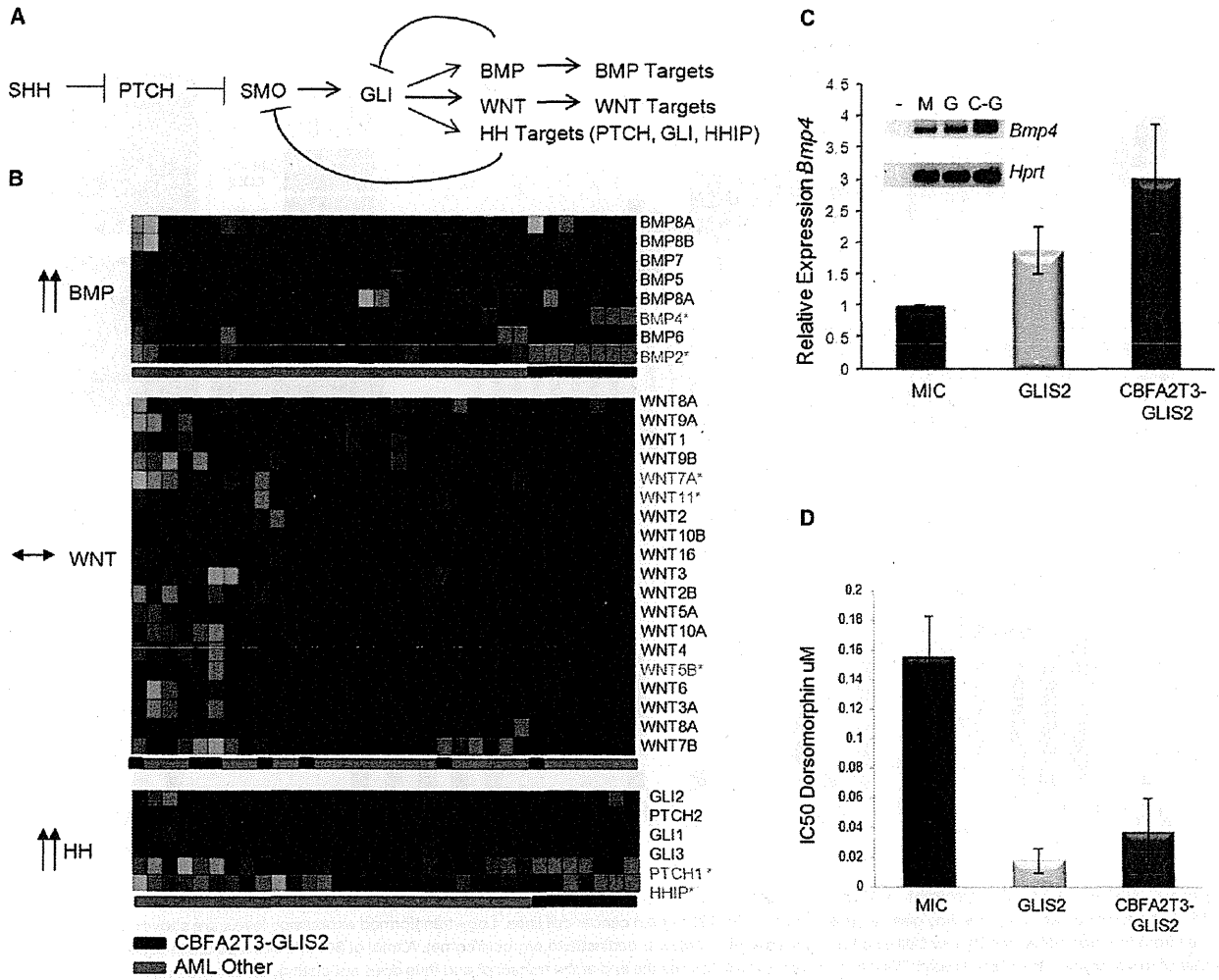

Figure 6. *CBFA2T3-GLIS2* Activates the BMP Pathway

(A) The Hedgehog (HH) signaling pathway. In addition to classic hedgehog targets such as *PTCH* and *HHIP*, *WNT* and *BMP* gene expression have been demonstrated to be affected by the GLI transcription factor in various models (Dahn and Fallon, 2000; Ingham and McMahon, 2001; Vokes et al., 2007).

(B) Gene expression profiles from *CBFA2T3-GLIS2* containing AMKL cases and other AML subtypes were evaluated for expression levels of *BMP*, *WNT*, and HH target genes. *CBFA2T3-GLIS2*-negative AMKL cases are not shown in this analysis. Significantly upregulated probe sets (FDR less than 0.05) are designated with red font: BMP2 FDR 1.06 × 10–17, BMP4 FDR 0.015976, PTCH1 FDR 2.05 × 10–6, and HHIP FDR 0.0038.

(C) Murine bone marrow cells were transduced with retroviral vectors carrying mCherry alone (MIC), mCherry plus *GLIS2*, or *CBFA2T3-GLIS2*. mCherry-positive cells were sorted and plated in methylcellulose containing IL3, IL6, SCF, and EPO. Following 1 week of growth, RNA was isolated, reverse transcribed, and amplified with *Bmp4* or *Hprt*-specific primers. Error bars represent mean ± SEM of four independent experiments. A representative gel is shown (–, neg; M, MIC; G, *GLIS2*; C-G, *CBFA2T3-GLIS2*). p = 0.047 as determined by one-way ANOVA.

(D) *GLIS2* and *CBFA2T3-GLIS2* sensitize murine hematopoietic cells to BMP receptor type I inhibition. Colony-formation assays were conducted in the presence or absence of dorsomorphin at the indicated concentrations (Yu et al., 2008). IC_{50} values were calculated as the amount of drug required to inhibit 50% of the colony formation as determined by colony counts. Error bars represent mean ± SEM of two independent experiments. p = 0.036 as determined by one-way ANOVA. See also Figure S4.

biological differences between pediatric and adult AMKL. Importantly, each of the detected chimeric transcripts is predicted to encode a fusion protein that would alter signaling pathways known to play a role in normal hematopoiesis, suggesting that these lesions are "driver" mutations that directly contribute to the development of leukemia. In addition to these somatic

(D) Colony morphology detected in *GLIS2* and *CBFA2T3-GLIS2*-modified cells from the second plating and beyond. a, CFU-Meg; b, CFU-GM. Scale bars, 500 μm. Representative cytospins and morphology of each colony type are shown. c, CFU-Meg; d, CFU-GM. Scale bars, 50 μm.

(E) Cells harvested from colony-forming assays after three or more replatings were subjected to flow cytometry. Cells were negative for acetylcholinesterase (data not shown).

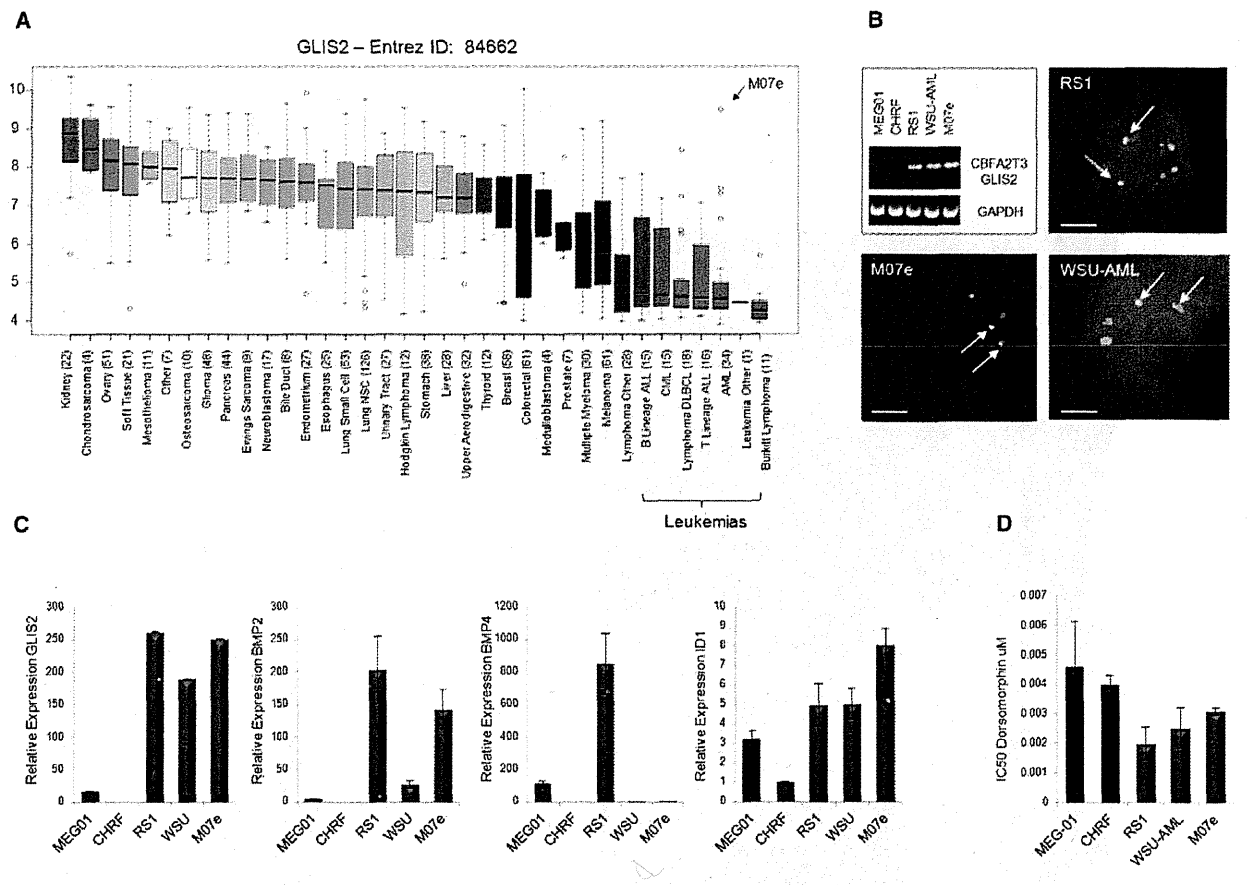

Figure 7. *CBFA2T3-GLIS2* Is Present in AMKL Cell Lines

(A) *GLIS2* expression as determined by gene expression arrays in 991 human cancer cell lines. Log_2-transformed expression levels are shown. Data were obtained from the Broad-Novartis Cancer Cell Line Encyclopedia (http://www.broadinstitute.org/ccle/home). A total of 34 AML cell lines are included; the extreme outlier of this subtype, M07e, is indicated. The *GLIS2* probe set recognizes the end of the transcript and thus does not distinguish between wild-type *GLIS2* and *CBFA2T3-GLIS2*. Median values are indicated by the band within the box plots; the ends of the whiskers indicate upper and lower adjacent values. Outliers are denoted by open circles.

(B) RT-PCR on five AMKL cell lines: MEG-01, CHRF-288-11, RS-1, WSU-AML, and M07e. The three cell lines carrying *CBFA2T3-GLIS2* were validated by FISH. Scale bars, 10 μm.

(C) Real-time semiquantitative RT-PCR of *GLIS2*, *BMP2*, *BMP4*, and *ID1* on the five AMKL cell lines. Expression levels relative to β-actin are shown. CHRF-288-11 expression levels were set to one (1) for comparison across cell lines. Error bars represent mean ± SEM of two independent experiments.

(D) Dorsomorphin sensitivity in the cell lines as determined by MTT assay. Error bars represent mean ± SEM of two independent experiments. For cell line information and MTT assay, please see Supplemental Experimental Procedures.

structural alterations, a variety of other somatic mutations were detected, including activating mutations in kinase signaling pathways in 21.6% of cases (*JAK* kinase family members and *MPL*), inactivating mutations in *GATA1* in 9.8% of cases, and amplification of chromosome 21 in the DSCR that includes genes known to play a role in AML such as *RUNX1*, *ETS2*, and *ERG* in 50% of the cases. How these mutations interact to not only induce overt leukemia but also to influence therapeutic responses remains to be determined.

As part of the St. Jude Children's Research Hospital-Washington University Pediatric Cancer Genome Project, we have sequenced 260 cases of pediatric cancers across multiple tumor types (Downing et al., 2012). The CBFA2T3-GLIS2 fusion was limited to AMKL cases. This specificity may exist for several reasons. The N-terminal portion of the fusion, CBFA2T3, is primarily expressed in the hematopoietic compartment, leading one to predict that expression of the inversion product, if it were to occur, would primarily be limited to hematopoietic cells. Although we do not know the exact target cell of transformation, induction of BMP4 signaling in human CD34+ progenitors has been demonstrated to increase the percentage of megakaryocyte and erythroid colonies in vitro (Fuchs et al., 2002; Jeanpierre et al., 2008). Thus, enhanced BMP signaling as a result of the expression of the inv(16)-encoded CBFA2T3-GLIS2 may directly contribute to the megakaryocytic differentiation of the leukemia cells.

The inv(16)-encoded *CBFA2T3-GLIS2* chimeric gene induced aberrant high-level expression of the DNA-binding domain of

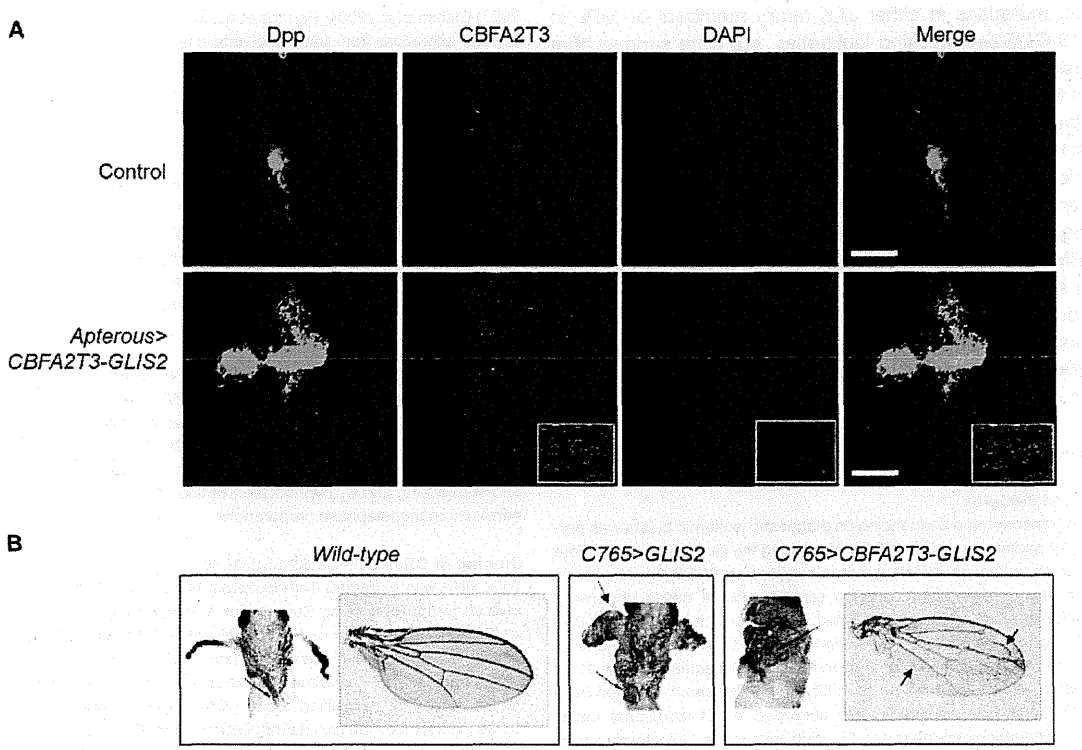

Figure 8. Transgenic *CBFA2T3-GLIS2 Drosophila* Ectopically Expresses Dpp

(A) *CBFA2T3-GLIS2* was expressed under control of *Apterous-Gal4* (strong epithelial dorsal driver). *dpp-lacZ* serves as a reporter for *dpp* induction. Wing imaginal discs were isolated at the late third instar, stained for β-gal as a readout for dpp (green), CBFA2T3 (red), and DAPI (blue), followed by immunofluorescence analysis. Nuclear localization of CBFA2T3-GLIS2 can be seen by the pink signal (inset). Scale bars, 100 μm.

(B) *CBFA2T3-GLIS2* was expressed under control of C765, a weak epithelial driver. Pharate adults were dissected from pupal casings and imaged. Arrows indicate ectopic notum, broadened and shortened legs. No *C765 > GLIS2 Drosophila* matured to adulthood. Arrows indicate ectopic veins in wings of rare *C765 > CBFA2T3-GLIS2* escapers.

See also Figure S5.

GLIS2 in hematopoietic cells, along with the disruption of one allele of *CBFA2T3*, a gene whose encoded protein has been shown to play a role in maintaining normal hematopoietic stem cell quiescence (Chyla et al., 2008). GLIS2 is a distant member of the GLI superfamily of transcriptional factors that function as critical transcriptional targets of the SHH signaling pathway (Hui and Angers, 2011). Although alterations in the SHH pathway have been directly implicated in a range of cancers (Barakat et al., 2010), the role of SHH signaling in normal hematopoiesis and leukemia remains poorly defined (Lim and Matsui, 2010). Our data suggest that aberrant expression of GLIS2 results in upregulation of the classic SHH-negative feedback inhibitors PTCH and HHIP, coupled with a marked increase in the expression of BMP 2 and 4, resulting in enhanced BMP signaling. These results indicate that CBFA2T3-GLIS2 functions, in part, as a gain-of-function GLIS2 allele. The exact mechanisms by which GLIS2 induced the upregulation of BMP2/BMP4 remains incompletely defined, although our data suggest that a direct transcription effect of GLIS2 on the BMP4 promoter is likely, although an indirect mechanism may also contribute.

Interestingly, BMP4 has been shown to expand and maintain human cord blood hematopoietic stem cells in vitro both directly, as well as indirectly via SHH signaling (Bhardwaj et al., 2001; Bhatia et al., 1999). Furthermore, *ID1*, a downstream BMP target previously implicated in leukemogenesis, was found to be upregulated in *CBFA2T3-GLIS2*-modified hematopoietic cells, demonstrating that this pathway is activated (Wang et al., 2011). Consistent with these findings, we demonstrated that activation of BMP signaling contributed to the marked increase in the replating capacity of myeloid/erythroid-committed progenitors. Accordingly, we found that murine hematopoietic cells carrying either full-length *GLIS2*, or *CBFA2T3-GLIS2*, demonstrated an increased sensitivity to BMP inhibition, suggesting that upregulation of this pathway contributes to the observed phenotype. In addition, BMP4 signaling has been shown to induce the differentiation of human CD34+ progenitors into megakaryocytes (Jeanpierre et al., 2008), suggesting that the upregulation of this pathway is also contributing to the megakaryocyte differentiation phenotype of these leukemias. Finally, BMP4, like thrombopoietin, appears to exert its effects on human megakaryopoiesis in part through the JAK/STAT pathways (Jeanpierre et al., 2008). Interestingly, functional pathway analysis of gene expression profiles in *CBFA2T3-GLIS2*-positive AMKL samples identified genes in the Jak-STAT signaling pathway to be significantly upregulated ($p = 0.0038$; FDR 0.022978; Figure S4). Combined with the identification in some cases of

activating mutations in either JAK family members or MPL in *CBFA2T3-GLIS2*-expressing leukemias, our data suggest that these lesions likely cooperate in leukemogenesis.

Taken together, these data define a poor prognostic subgroup of pediatric AMKL patients that are characterized by the inv(16)(p13.3q24.3)-encoded CBFA2T3-GLIS2 fusion protein. Expression of *CBFA2T3-GLIS2* induces an enhanced replating capacity of lineage-committed myeloid progenitors, along with megakaryocytic differentiation, in part through enhanced BMP2/BMP4 signaling. Whether altered SHH and CBFA2T3-induced signaling also contributes to leukemogenesis remains to be determined. Nevertheless, the presented data raise the important possibility that inhibition of the BMP pathway may have a therapeutic benefit in this aggressive form of pediatric AML.

EXPERIMENTAL PROCEDURES

Patients and Samples

Paired-end transcriptome sequencing on diagnostic leukemic blasts was performed on 14 pediatric non-DS-AMKL cases using the Illumina platform. Four of these cases underwent whole-genome sequencing (WGS) on diagnostic leukemia blasts and matched germline samples. All 14 cases underwent whole-exome sequencing for which 10 had matching germline samples. One additional diagnostic sample with matched germline DNA had whole-exome sequencing done that did not undergo transcriptome sequencing. All 15 of these patients were treated at St Jude Children's Research Hospital from 1990 to 2008. The recurrence cohort consisted of 61 additional cases including 33 pediatric specimens and 28 adult specimens . All samples were obtained with patient or parent/guardian-provided informed consent under protocols approved by the Institutional Review Board at each institution and St. Jude Children's Research Hospital.

Sequencing

RNA and DNA library construction for transcriptome and whole-genome DNA sequencing, respectively, has been described previously (Mardis et al., 2009; Zhang et al., 2012). Analysis of WGS data and whole-exome sequencing data that include mapping, coverage and quality assessment, single-nucleotide variant (SNV)/Indel detection, tier annotation for sequence mutations, prediction of deleterious effects of missense mutations, and identification of loss of heterozygosity was described previously (Zhang et al., 2012). Please see Supplemental Experimental Procedures for details.

Recurrency Screening for Sequence Variations and Fusions

We performed recurrence screening on a cohort of 61 AMKL samples. All 61 were screened by RT-PCR (see Supplemental Experimental Procedures for primers and conditions) for *CBFA2T3-GLIS2*, *GATA2-HOXA9*, *MN1-FLI1*, *NIPBL-HOXB9*, and *NUP98-KDM5A*. Whole-genome-amplified DNA (QIAGEN) from 38 cases underwent PCR and Sanger sequencing by Beckman Coulter Genomics for *JAK1*, *JAK2*, *JAK3*, and *MPL* mutations. In 8 of 38 cases, a paired matched germline was available. Putative SNVs and indel variants were detected by SNPdetector (Zhang et al., 2005).

Overall Survival Probabilities

Outcome data were available for 40 pediatric patients tested for *CBFA2T3-GLIS2*. *CBFA2T3-GLIS2* was found in 13 patients. Overall survival was defined as the date of diagnosis or study enrollment to the date of death with surviving patients censored at the date of last follow-up. Survival curves were estimated using the Kaplan-Meier method and compared using the exact log rank test based on 10,000 permutations.

Affymetrix SNP Array

Affymetrix SNP 6.0 array genotyping was performed for 14 of 15 AMKL cases in the discovery cohort, and array normalization and DNA copy number alterations were identified as previously described (Lin et al., 2004; Mullighan et al., 2007; Olshen et al., 2004; Pounds et al., 2009). To differentiate inherited copy number alterations from somatic events in leukemia blasts from patients lacking matched normal DNA, identified putative variants were filtered using public copy number polymorphism databases and a St. Jude database of SNP array data from several hundred samples (Iafrate et al., 2004; McCarroll et al., 2008).

Gene Expression Profiling

Gene expression profiling was performed using Affymetrix Human Exon 1.0 ST Arrays (Affymetrix) according to manufacturer's instructions. This cohort comprised 39 pediatric AML samples including AMKL (n = 14), *AML1-ETO* (n = 4), *CBFB-MYH11* (n = 2), *MLL* rearranged (n = 3), *PML-RARA* (n = 2), *NUP98-NSD1* (n = 2), *HLXB9-ETV6* (n = 1), and AML cases lacking chimeric genes (n = 11). Please see Supplemental Experimental Procedures for further details.

FISH

Dual-color FISH was performed on archived bone marrow cells and cell lines as described previously by Mullighan et al. (2007). Probes were derived from bacterial artificial chromosome (BAC) clones (Invitrogen). BACs used were RP11-830F9 (*CBFA2T3*), CTD-25555M20 (*GLIS2*), RP11-345E21 (*MN1*), and CTD-2542E23 (*FLI1*). BAC clone identity was verified by T7 and SP6 BAC-end sequencing and by hybridization of fluorescently labeled BAC DNA with normal human metaphase preparations.

Cloning of CBFA2T3-GLIS2 and GLIS2

Total RNA was extracted from leukemia blasts using RNeasy (QIAGEN) and reverse transcribed using Superscript III (Invitrogen) as per manufacturer's instructions. The coding region of *CBFA2T3-GLIS2* was PCR amplified from patient M712 and M707 using primers CBFA2T3_119F and GLIS2_1685R (see Supplemental Experimental Procedures for primers and conditions). *GLIS2* was PCR amplified from cDNA using primers GLIS2_21F and GLIS2_1685R (see Supplemental Experimental Procedures for primers and conditions). PCR products were subcloned into the pGEM-T Easy Vector (Promega) and sequenced. Clones containing the correct sequence were then subcloned into the MIC retroviral backbone (Volanakis et al., 2009).

Murine Bone Marrow Transduction and Colony-Forming Assays

All experiments involving mice were reviewed and approved by the Institutional Animal Care and Use Committee. Bone marrow from 4- to 6-week-old female C57/BL6 mice was harvested and cultured in the presence of recombinant murine SCF (rmSCF), IL3 (rmIL3), and IL6 (rmIL6) (Peprotech; all 50 ng/ml) for 24 hr prior to transduction on RetroNectin (Takara Bio)-coated plates. Ecotropic envelope-pseudotyped retroviral supernatant was produced by transient transfection of 293T cells as previously described by Soneoka et al. (1995). Forty-eight hours following transduction, cells were harvested, sorted for mCherry expression, and plated on methylcellulose containing IL3, IL6, SCF, and EPO (Stem Cell Technologies, Vancouver, British Columbia, Canada) as per manufacturer's instructions. Colonies were counted after 7 days of growth at 37°C, harvested, and replated. In a subset of experiments, dorsomorphin (Sigma-Aldrich) was added to the methylcellulose at the indicated concentrations.

Flow Cytometry

Cells were resuspended in PBS and preincubated with anti-CD16/CD32 Fc-block (BD PharMingen) if staining did not include conjugated anti-murine CD16/32. Aliquots were stained for 15 min at 4°C with conjugated antibodies. Cells were washed and resuspended in DAPI containing solution (1 μg/ml DAPI in PBS) for subsequent analysis using FACS LSR II D (BD Biosciences). For a list of antibodies used, please see Supplemental Experimental Procedures.

Luciferase Assays

The human BMP4 promoter-driven luciferase construct pSLA4.1EX (Van den Wijngaard et al., 1999) was kindly provided by E. Joop van Zoelen, Nijmegen, The Netherlands. The murine BMP response element (pBRE) (Korchynskyi and ten Dijke, 2002) was kindly provided by Peter ten Dijke, Leiden, The Netherlands. The 8 × 3′ Gli-BS luciferase reporter (pGli-BS) (Sasaki et al., 1997) has been previously described. TOPFlash and FOPFlash (Korinek et al., 1997) constructs were obtained from Addgene. For details on luciferase reporter assays, please see Supplemental Experimental Procedures.

ELISA

BMP4 protein levels in the supernatants from transduced murine hematopoietic cells were determined by ELISA. Briefly, mCherry-positive bone marrow cells transduced with empty (MIC), GLIS2, or CBFA2T3-GLIS2-containing retroviruses were placed in media containing IL3, IL6, and SCF for 48 hr, and supernatant was then harvested and the level of murine BMP4 determined using an ELISA kit purchased from TSZELISA (http://www.tszelisa.com). Measurements were done according to manufacturer's instructions.

Transgenic *Drosophila*

CBFA2T3-GLIS2 and *GLIS2* cDNAs were subcloned into the *pUAS-attB* plasmid (Bischof et al., 2007). Transgenic UAS-*CBFA2T3-GLIS2* and UAS-*GLIS2* flies were generated using site-specific ϕC31 integration system (Bischof et al., 2007). Embryo injections were performed by Best Gene. UAS constructs were targeted to chromosome 2R-51D in order to avoid differential positional effects on transgene expression. For wing imaginal disc staining, relevant crosses were performed to generate flies carrying all three transgenes: *Apterous-Gal4* (a strong epithelial dorsal compartment-specific GAL4 driver), UAS-*CBFA2T3-GLIS2*, and a *dpp-lacZ* enhancer trap reporter. Gal4 driver and *dpp-lacZ* reporter stocks were obtained from the Bloomington Stock Center. Wing imaginal discs were dissected from wandering third-instar larvae, fixed, and immunostained using anti-β-gal (Promega; Z378), anti-CBFA2T3 (Abcam; ab33072), and DAPI (Invitrogen; D3571) as previously described by Carroll et al. (2012). To assess the phenotypic effects of *CBFA2T3-GLIS2* and *GLIS2*, UAS transgenes were expressed under control of the epithelial driver *C765-Gal4*, and progeny was observed. Pharate adults were dissected from pupal casings and imaged.

ACCESSION NUMBERS

The sequence data and SNP microarray data have been deposited in the dbGaP database (http://www.ncbi.nlm.nih.gov/gap) under the accession number phs000413.v1.p1. Affymetrix gene expression data have been deposited in the NCBI Gene Expression Omnibus (http://www.ncbi.nlm.nih.gov/geo/) under GSE35203.

SUPPLEMENTAL INFORMATION

Supplemental Information includes five figures, seven tables, and Supplemental Experimental Procedures and can be found with this article online at http://dx.doi.org/10.1016/j.ccr.2012.10.007.

ACKNOWLEDGMENTS

The authors would like to specifically thank Joy Nakitandwe for critical input and discussions, Susana Raimondi for review of cytogenetics, Matt Stine for assistance with data deposition, Bill Pappas and Scott Malone for support of the information technology infrastructure, and the staff of Tissue Resources Laboratory, Flow Cytometry and Cell Sorting Core, the Hartwell Center for Biotechnology and Bioinformatics of St Jude Children's Research Hospital, and Emily Dolezale for assistance in sample procurement at Memorial Sloan Kettering Cancer Center. This work was supported by grants from the National Institutes of Health (Cancer Center Support Grant P30 CA021765), the Eric Trump Foundation, a Leukemia & Lymphoma Society Specialized Center of Research Grant LLS7015, and the American Lebanese Syrian Associated Charities (ALSAC) of St Jude Children's Research Hospital.

Received: June 21, 2012
Revised: September 5, 2012
Accepted: October 17, 2012
Published: November 12, 2012

REFERENCES

Argiropoulos, B., and Humphries, R.K. (2007). Hox genes in hematopoiesis and leukemogenesis. Oncogene *26*, 6766–6776.

Athale, U.H., Razzouk, B.I., Raimondi, S.C., Tong, X., Behm, F.G., Head, D.R., Srivastava, D.K., Rubnitz, J.E., Bowman, L., Pui, C.H., and Ribeiro, R.C. (2001). Biology and outcome of childhood acute megakaryoblastic leukemia: a single institution's experience. Blood *97*, 3727–3732.

Attanasio, M., Uhlenhaut, N.H., Sousa, V.H., O'Toole, J.F., Otto, E., Anlag, K., Klugmann, C., Treier, A.C., Helou, J., Sayer, J.A., et al. (2007). Loss of GLIS2 causes nephronophthisis in humans and mice by increased apoptosis and fibrosis. Nat. Genet. *39*, 1018–1024.

Barakat, M.T., Humke, E.W., and Scott, M.P. (2010). Learning from Jekyll to control Hyde: Hedgehog signaling in development and cancer. Trends Mol. Med. *16*, 337–348.

Barnard, D.R., Alonzo, T.A., Gerbing, R.B., Lange, B., and Woods, W.G.; Children's Oncology Group. (2007). Comparison of childhood myelodysplastic syndrome, AML FAB M6 or M7, CCG 2891: report from the Children's Oncology Group. Pediatr. Blood Cancer *49*, 17–22.

Barretina, J., Caponigro, G., Stransky, N., Venkatesan, K., Margolin, A.A., Kim, S., Wilson, C.J., Lehár, J., Kryukov, G.V., Sonkin, D., et al. (2012). The Cancer Cell Line Encyclopedia enables predictive modelling of anticancer drug sensitivity. Nature *483*, 603–607.

Bhardwaj, G., Murdoch, B., Wu, D., Baker, D.P., Williams, K.P., Chadwick, K., Ling, L.E., Karanu, F.N., and Bhatia, M. (2001). Sonic hedgehog induces the proliferation of primitive human hematopoietic cells via BMP regulation. Nat. Immunol. *2*, 172–180.

Bhatia, M., Bonnet, D., Wu, D., Murdoch, B., Wrana, J., Gallacher, L., and Dick, J.E. (1999). Bone morphogenetic proteins regulate the developmental program of human hematopoietic stem cells. J. Exp. Med. *189*, 1139–1148.

Bischof, J., Maeda, R.K., Hediger, M., Karch, F., and Basler, K. (2007). An optimized transgenesis system for *Drosophila* using germ-line-specific phiC31 integrases. Proc. Natl. Acad. Sci. USA *104*, 3312–3317.

Buijs, A., van Rompaey, L., Molijn, A.C., Davis, J.N., Vertegaal, A.C., Potter, M.D., Adams, C., van Baal, S., Zwarthoff, E.C., Roussel, M.F., and Grosveld, G.C. (2000). The MN1-TEL fusion protein, encoded by the translocation (12;22)(p13;q11) in myeloid leukemia, is a transcription factor with transforming activity. Mol. Cell. Biol. *20*, 9281–9293.

Carroll, A., Civin, C., Schneider, N., Dahl, G., Pappo, A., Bowman, P., Emami, A., Gross, S., Alvarado, C., Phillips, C., et al. (1991). The t(1;22) (p13;q13) is nonrandom and restricted to infants with acute megakaryoblastic leukemia: a Pediatric Oncology Group Study. Blood *78*, 748–752.

Carroll, C.E., Marada, S., Stewart, D.P., Ouyang, J.X., and Ogden, S.K. (2012). The extracellular loops of Smoothened play a regulatory role in control of Hedgehog pathway activation. Development *139*, 612–621.

Chyla, B.J., Moreno-Miralles, I., Steapleton, M.A., Thompson, M.A., Bhaskara, S., Engel, M., and Hiebert, S.W. (2008). Deletion of Mtg16, a target of t(16;21), alters hematopoietic progenitor cell proliferation and lineage allocation. Mol. Cell. Biol. *28*, 6234–6247.

Creutzig, U., Reinhardt, D., Diekamp, S., Dworzak, M., Stary, J., and Zimmermann, M. (2005). AML patients with Down syndrome have a high cure rate with AML-BFM therapy with reduced dose intensity. Leukemia *19*, 1355–1360.

Dahn, R.D., and Fallon, J.F. (2000). Interdigital regulation of digit identity and homeotic transformation by modulated BMP signaling. Science *289*, 438–441.

Downing, J.R., Wilson, R.K., Zhang, J., Mardis, E.R., Pui, C.-H., Ding, L., Ley, T.J., and Evans, W.E. (2012). The Pediatric Cancer Genome Project. Nat. Genet. *44*, 619–622.

Fuchs, O., Simakova, O., Klener, P., Cmejlova, J., Zivny, J., Zavadil, J., and Stopka, T. (2002). Inhibition of Smad5 in human hematopoietic progenitors blocks erythroid differentiation induced by BMP4. Blood Cells Mol. Dis. *28*, 221–233.

Gamou, T., Kitamura, E., Hosoda, F., Shimizu, K., Shinohara, K., Hayashi, Y., Nagase, T., Yokoyama, Y., and Ohki, M. (1998). The partner gene of AML1 in t(16;21) myeloid malignancies is a novel member of the MTG8(ETO) family. Blood *91*, 4028–4037.